

THESIS

IDENTIFICATION AND CHARACTERIZATION OF DENDRITIC, PARALLEL, PINNATE, RECTANGULAR, AND TRELLIS NETWORKS BASED ON DEVIATIONS FROM PLANFORM SELF-SIMILARITY

Submitted by
Alfonso I. Mejía
Department of Civil and Environmental Engineering

In partial fulfillment of the requirements
For the Degree of Master of Science
Colorado State University
Fort Collins, Colorado
Fall 2006

COLORADO STATE UNIVERSITY

AUGUST 10, 2006

WE HEREBY RECOMMEND THAT THE THESIS PREPARED UNDER OUR SUPERVISION BY ALFONSO I. MEJÍA ENTITLED IDENTIFICATION AND CHARACTERIZATION OF DENDRITIC, PARALLEL, PINNATE, RECTANGULAR, AND TRELLIS NETWORKS BASED ON DEVIATIONS FROM PLANFORM SELF-SIMILARITY BE ACCEPTED AS FULFILLING IN PART REQUIREMENTS FOR THE DEGREE OF MASTER OF SCIENCE.

Committee on Graduate Work

Ellen Work

Ellen Work
Jorge A. Ramirez

JORGE A RAMIREZ

Jeffrey D. Niemann
Advisor

Luis Garcia
Department Head

ABSTRACT OF THESIS

IDENTIFICATION AND CHARACTERIZATION OF DENDRITIC, PARALLEL, PINNATE, RECTANGULAR, AND TRELLIS NETWORKS BASED ON DEVIATIONS FROM PLANFORM SELF-SIMILARITY

Geomorphologists have long recognized that the geometry of channel network planforms can vary significantly between regions depending on the local lithologic and tectonic conditions. This tendency has led to the classification of channel networks using terms such as dendritic, parallel, pinnate, rectangular, and trellis. Unfortunately, available classification methods are scale dependent and have no connection to an underlying quantitative theory of drainage network geometry or evolution. In this study, a new method is developed to classify drainage networks based on their deviations from self-similarity. The planform geometry of dendritic networks is known to be self-similar. It is our hypothesis that parallel, pinnate, rectangular, and trellis networks correspond to distinct deviations from this self-similarity. To identify such deviations, three measures of channel networks are applied to ten networks from each classification. These measures are the incremental accumulation of drainage area along channels, the irregularity of channel courses, and the angles formed by merging channels. The results confirm and characterize the self-similarity of dendritic networks. Parallel and pinnate networks are found to be self-affine with Hurst exponents around 0.8 and 0.7,

respectively. Rectangular and trellis networks are approximately self-similar although deviations from self-similarity are observed. Rectangular networks have more sinuous channels than dendritic networks across all scales, and trellis networks have a slower rate of area accumulation than dendritic networks across all scales. Such observations are used to build and test classification trees, which are found to perform well in classifying networks.

Alfonso I. Mejía
Civil and Environmental Engineering Department
Colorado State University
Fort Collins, CO 80523
Fall 2006

ACKNOWLEDGMENTS

The financial support of the U.S. Army Research Office Terrestrial Sciences Program is gratefully acknowledged. Special acknowledgment and gratitude is expressed to Jeff Niemann for all the support, motivation, guidance, insights, and ideas provided during the course of this research. Acknowledgment and gratitude is also expressed to José D. Salas for all the guidance and support offered during the course of the master.

DEDICATION

A mis viejos. A mi viejo por la carga de sueño, aliento, y compromiso que siempre me ha sabido brindar. A mi vieja por lo del amor sin condiciones y la dedicación sin tramos. El agradecimiento a ambos es sin límites.

“De la pensée discursive ou de l'ellipse poétique, qui va plus loin et de plus loin? Et de cette nuit originelle où tâtonnent deux aveugles-nés, l'un équipé de l'outillage scientifique, l'autre assisté des seules fulgurations de l'intuition, qui donc plus tôt remonte, et plus chargé de brève phosphorescence. La réponse n'importe. Le mystère est commun.”
[Perse, 1960]

TABLE OF CONTENTS

ABSTRACT OF THESIS	iii
ACKNOWLEDGMENTS	v
DEDICATION	vi
1 Introduction.....	10
2 Planform Self-similarity.....	19
2.1 Drainage Area Increments.....	22
2.2 Stream Course Irregularity	25
2.3 Tributary Junction Angles.....	27
3 Dataset.....	31
4 Results	36
4.1 Selection of Ruler Factor.....	36
4.2 Dendritic Networks	37
4.3 Parallel Networks	39
4.4 Pinnate Networks	41
4.5 Rectangular Networks	42
4.6 Trellis Networks	44
5 Classification Method	53
6 Conclusions.....	62
References	64

LIST OF TABLES

Table 3.1. Basins analyzed including the author who previously classified the basin....35

LIST OF FIGURES

Figure 1.1. Examples of the five network classifications analyzed in this paper. The dots in the figure identify the basin outlets. 18

Figure 2.1. Illustration of the measurement of (a) the drainage area increments, (b) the stream course irregularity, and (c) the junction angles. 30

Figure 4.1. Plots of the average values of (a) $\Delta A_{bL}(L)/L^2$, (b) $\sigma_{bL}(L)/L$, and (c) $\psi_{bL,bL_1}(L)$ as a function of basin size L when different values of b are used on a dendritic network (Turkey Creek). The lines in (c) have been offset as indicated in the figure for clarity..... 46

Figure 4.2. Plots of the average values of (a) $\Delta A_{bL}(L)/L^2$, (b) $\sigma_{bL}(L)/L$, and (c) $\psi_{bL,bL_1}(L)$ as a function of basin size L for four typical dendritic networks. The dashed lines show the regression lines fit to the plots of the average values. The lines for the different basins have been offset as indicated in the figure for clarity..... 47

Figure 4.3. Plots of the average values of (a) $\Delta A_{bL}(L)/L^2$, (b) $\sigma_{bL}(L)/L$, and (c) $\psi_{bL,bL_1}(L)$ as a function of basin size L for four typical parallel networks. The dashed lines show the regression lines fit to the plots of the average values. The lines for the different basins have been offset as indicated in the figure for clarity..... 48

Figure 4.4. Impact of restricting range of tributary sizes used to calculate $\psi_{bL,bL_t}(L)$. In (a), the allowable range of secondary tributary sizes is $0 < L_t < L$. In (b), the allowable range is $0.6L < L_t < 1.0L$ 49

Figure 4.5. Plots of the average values of (a) $\Delta A_{bL}(L)/L^2$, (b) $\sigma_{bL}(L)/L$, and (c) $\psi_{bL,bL_t}(L)$ as a function of basin size L for four typical pinnate networks. The dashed lines show the regression lines fit to the plots of the average values. The lines for the different basins have been offset as indicated in the figure for clarity..... 50

Figure 4.6. Plots of the average values of (a) $\Delta A_{bL}(L)/L^2$, (b) $\sigma_{bL}(L)/L$, and (c) $\psi_{bL,bL_t}(L)$ as a function of basin size L for four typical rectangular networks. The dashed lines show the regression lines fit to the plots of the average values. The lines for the different basins have been offset as indicated in the figure for clarity..... 51

Figure 4.7. Plots of the average values of (a) $\Delta A_{bL}(L)/L^2$, (b) $\sigma_{bL}(L)/L$, and (c) $\psi_{bL,bL_t}(L)$ as a function of basin size L for four typical trellis networks. The dashed lines show the regression lines fit to the plots of the average values. The lines for the different basins have been offset as indicated in the figure for clarity. 52

Figure 5.1. Summary of the average value, slope, and residual variance obtained for the drainage area increments. 58

Figure 5.2. Summary of the average value, slope, and residual variance obtained for the stream course irregularity. 59

Figure 5.3. Summary of the average value, slope, and residual variance obtained for the tributary junction angles. 60

Figure 5.4. (a) Automatically-generated and (b) conceptual classification trees derived from all 50 basins analyzed in this paper. 61

1 Introduction

Geomorphologists have long recognized that channel networks can appear quite distinct between different regions. Usually channel networks appear tree-like with irregular stream courses and tributaries that form acute angles at their junctions [*Zernitz*, 1932]. In some cases, however, channel networks can have rather different properties. For example, some networks appear lattice-like with tributaries joining at nearly right angles and channels oriented primarily in two orthogonal directions [*Howard*, 1967]. In other cases, networks appear more feather-like with many short tributaries joining the major channels at regular intervals [*Parvis*, 1950].

These differences have led geomorphologists to develop classification systems for channel networks. The first classification system was proposed by *Zernitz* [1932] based on inspection of channel network geometry on maps. This classification system is two tiered with a set of basic patterns and a set of modified patterns. Patterns are considered basic if they exhibit a distinct set of characteristics from other basic patterns. Modified patterns exhibit some similarities to a particular basic pattern but also some differences. *Parvis* [1950] expanded this classification system by introducing fifteen new modified patterns based on an analysis of aerial photos. *Howard* [1967] further expanded the classification system by introducing two new basic patterns, seven modified patterns, and a third tier of classification called drainage varieties. In his view, modified patterns can be distinguished based on larger-scale regional characteristics while drainage varieties are

distinguished based on smaller-scale internal characteristics of the networks. He suggested that the actual number of drainage varieties in nature could be quite large because of the level of detail used to distinguish them. These classifications are now widely reproduced, at least in part, in introductory geomorphology and physical geology textbooks [*Gregory and Walling, 1973; Plummer and McGeary, 1993; Knighton, 1998*].

Classifications consider either disconnected, distributional, or aggregating networks. Disconnected networks do not exhibit continuously-connected channels from the stream sources to the edges of the region. Disconnected patterns include the so-called multibasinal and collinear networks. Distributional patterns, such as radial and distributary, tend to distribute flow from a relatively small number of sources to a relatively large number of outlets at the edge of the region. Aggregating networks tend to collect water from many sources and transport it to relatively few outlets.

In this study, we focus on a set of classifications for aggregating patterns, specifically the dendritic, parallel, pinnate, rectangular, and trellis classifications. Figure 1.1 shows examples of these network types. A dendritic network is tree-like with balanced branching among channels of different sizes, somewhat irregular stream courses, channels oriented in many directions, and tributaries that merge at acute angles [*Zernitz, 1932; Parvis, 1950; Howard, 1967*]. A parallel network has stream courses that tend to be very straight, major channels that tend to be parallel, and tributaries that merge at very acute angles [*Zernitz, 1932; Parvis, 1950; Howard, 1967*]. A pinnate network appears feather-like with a major channel that tends to be very straight and aligned in a single direction and many small tributaries joining the major channel at regular intervals and acute angles [*Zernitz, 1932; Parvis, 1950; Howard, 1967*]. In a rectangular network,

channel sinuosity is introduced by a large number of right angle bends and tributaries that sometimes merge at nearly right angles [Zernitz, 1932; Howard, 1967]. Finally, a trellis network appears lattice-like because small channels tend to be numerous and short in comparison to the large channels. Channel sinuosity is low, and tributaries often merge at nearly right angles [Zernitz, 1932; Howard, 1967]. All of these classifications were considered basic patterns by Howard [1967] except for the pinnate classification, which was considered a modification of the dendritic pattern by Zernitz [1932] and Howard [1967], and a modification of the parallel pattern by Phillips and Schumm [1987].

Drainage pattern classifications are also thought to be related to the conditions under which the networks formed. Parvis [1950] developed his classification system as part of a process to infer soil and bedrock types from aerial photos. Howard [1967] compared the network characteristics with known geological properties of regions and concluded that the analysis of drainage patterns can provide useful information about structural features and the types of underlying materials. In fact, many researchers have documented relations between drainage patterns and underlying bedrock [Zernitz, 1932; Horton, 1945; Parvis, 1950; Howard, 1967; Abrahams and Flint, 1983], soils [Parvis, 1950], tectonics [Cox, 1989; Burbank, 1992], climate [Daniel, 1981], and erosional processes [Dunne, 1980]. Dendritic networks typically occur in regions with little tectonic control, gentle regional slopes, and relatively uniform lithology [Zernitz, 1932]. Parallel networks generally occur in regions with moderate to steep regional slopes or where elongated landforms such as drumlins restrict flow to parallel paths [Zernitz, 1932; Howard, 1967]. Phillips and Schumm [1987] used physical experiments to show that experimental channel networks can become parallel if they develop on surfaces with

initial slopes above 2-3%. Various explanations have been proposed for the origins of pinnate networks. *Zernitz* [1932] suggested that they occur when tectonic controls result in steep and uniform valley walls along the major channel. *Parvis* [1950] suggested that deep loess deposits tend to have low parallel ridges and valleys due to aeolian processes, and that these valleys may tend to fix the locations of the main channels and produce pinnate networks. *Phillips and Schumm* [1987] suggested that pinnate networks may occur when the regional slope is extremely steep. Rectangular patterns are produced by systems of joints and/or faults that meet at right angles. Joints and faults represent zones of weakness that the channels exploit during their growth [*Howard*, 1967]. Trellis patterns are commonly found in regions of folded or tilted strata where a series of parallel faults [*Parvis*, 1950] are present or in dissected, belted coastal plains [*Zernitz*, 1932].

Several authors have sought to quantify the differences between drainage network classifications using either the orientations of the channels or the angles formed by merging tributaries. Channel orientations are usually studied by constructing a histogram or rosette in which the magnitude for each direction is determined by the number of links or the total length of channel oriented in that direction [*Milton*, 1965]. *Morisawa* [1963] examined the orientations of first order *Strahler* [1957] streams for different network types. For dendritic networks, the distribution is nearly uniform. For parallel networks, the streams tend to be oriented in a single direction. For rectangular networks, the streams tend to be oriented in two approximately orthogonal directions. *Phillips and Schumm* [1987] analyzed the junction angles of several parallel networks in Colorado and Wyoming. They found that the junction angles among the major channels are typically around 40°, whereas the junction angles among lesser channels are typically about 61°.

Abrahams and Flint [1983] quantitatively analyzed both the stream orientations and junction angles of trellis networks. They found a preference for streams to be oriented in the down-dip and down-plunge directions and an increased occurrence of obtuse junction angles.

Methods have also been developed to classify networks using quantitative attributes. *Argialas et al.* [1988] proposed a quantitative classification method for third order networks. They digitized networks using aerial photos and maps and identified network elements such as the main stream, which they defined as the stream with the longest flow path, as well as the first, second, and third order Strahler streams. Strahler streams were further decomposed into links and nodes, where nodes are junctions or sources and links are stream segments that connect two nodes. Using this decomposition, they calculated approximately 15 attributes such as the source-outlet angle, which is the angle formed by a line from the center of gravity of the basin to the outlet and a line from the center of gravity to the main stream source. Then, the values of these attributes were classified into categories. For example, the source-outlet angle can be considered large or small, based on an empirical threshold of 105° [*Argialas et al.*, 1988]. These categories were then used in a classification tree to label a given network as either dendritic, parallel, pinnate, rectangular, trellis, angular, radial, or annular. Each of these network types consists of a unique combination of categories, which together define its place on the classification tree. *Argialas et al.* [1988] tested this classification method with twenty natural and artificial networks that were previously classified by visual inspection, and the method successfully classified all twenty networks. *Hadipriono et al.* [1990] developed an expert system to classify channel networks based on the method of

Argialas et al. [1988]. The expert system uses the same attributes and categories, but it also allows the user to incorporate their own qualitative observations into the classification process. *Ichoku and Chorowicz* [1994] proposed another quantitative classification method using digital elevation models (DEMs). This method can classify a network as either dendritic, parallel, pinnate, rectangular, or trellis based on 14 characteristics. Five of these characteristics are quantitative measurements, while the other nine are combinations of quantitative measurements and qualitative descriptions of the network. These characteristics are used in a classification tree with empirical thresholds to classify networks. For example, the first attribute that the classification tree considers is the mean length of exterior links. If the mean length is greater than 10 pixels, the network can be dendritic, parallel, rectangular, or remain unclassified. Otherwise, the network can be trellis, pinnate, or remain unclassified. *Ichoku and Chorowicz* [1994] do not state the method's rate of success in reproducing visual classifications, but they indicate that the method misclassifies networks that are much less than or greater than 6th order, especially if they are composed of several network types. For very small order networks, *Ichoku and Chorowicz* [1994] recommend the use of visual classification, and for large order networks, they recommend subdividing the network into smaller order networks to reduce misclassifications.

Although these methods objectively classify networks in a way that is consistent with visual inspection, they also have two significant weaknesses. First, the classification methods are scale dependent because they are designed for networks of a particular size. *Argialas et al.* [1988] explicitly considered 3rd order networks, while the method devised by *Ichoku and Chorowicz* [1994] works best for networks around 6th order. This

limitation can be problematic if the network of interest does not have the appropriate size. Furthermore, *Ichoku and Chorowicz* [1994] noted that the same network can be classified as rectangular or trellis if only the scale on the map is changed. Second, none of the available classification methods, whether visual or quantitative, are tied to an underlying quantitative theory of drainage network geometry or evolution [*Ichoku and Chorowicz*, 1994]. Quantitative methods, for example, require one to calculate large numbers of seemingly unrelated geometrical properties. As a result, it is difficult to establish quantitative connections between the drainage network types and the underlying tectonic and lithologic conditions. This lack of theory also leads to ambiguity in the classification hierarchy. For example, it is not clear why pinnate should be considered a modified pattern while contorted should be considered a basic pattern.

In this paper, we aim to distinguish different network types using a method that is more directly tied to an underlying theory for channel network geometry. In this approach, dendritic networks are considered as the single basic network type because they are known to develop when few topographic, lithological, and tectonic constraints impact the development of the network. Such networks have also been observed to conform to a type of planform self-similarity [*Rodríguez-Iturbe et al.*, 1992; *Peckham*, 1995; *Rigon et al.*, 1996; *Dodds and Rothman*, 1999; *Veneziano and Niemann*, 2000a, 2000b; *Niemann and Hasbargen*, 2005], which has been directly linked to a broad class of fluvial erosion models [*Veneziano and Niemann*, 2000a]. The central hypothesis of this paper is that parallel, pinnate, rectangular, and trellis networks represent distinct deviations from self-similarity that can be captured with relatively few measures. These particular network types are considered for two reasons. First, they all describe

aggregating patterns and can be identified by considering a single network and its sub-networks. Second, these patterns are relatively common in nature, so numerous examples of each type can be readily identified. In the next section (Section 2), we describe the planform self-similarity condition that applies to dendritic networks and develop three measures of drainage networks using this condition (drainage area increments, stream course irregularity, and tributary junction angles). Section 3 contains a discussion of the dataset used in this analysis including the process used to identify the channel networks. In Section 4, we describe the main results obtained using these measures for the various network types. In Section 5, we develop simple classification methods based on these measures and evaluate their performance. Finally, Section 6 contains the main conclusions from the analysis.

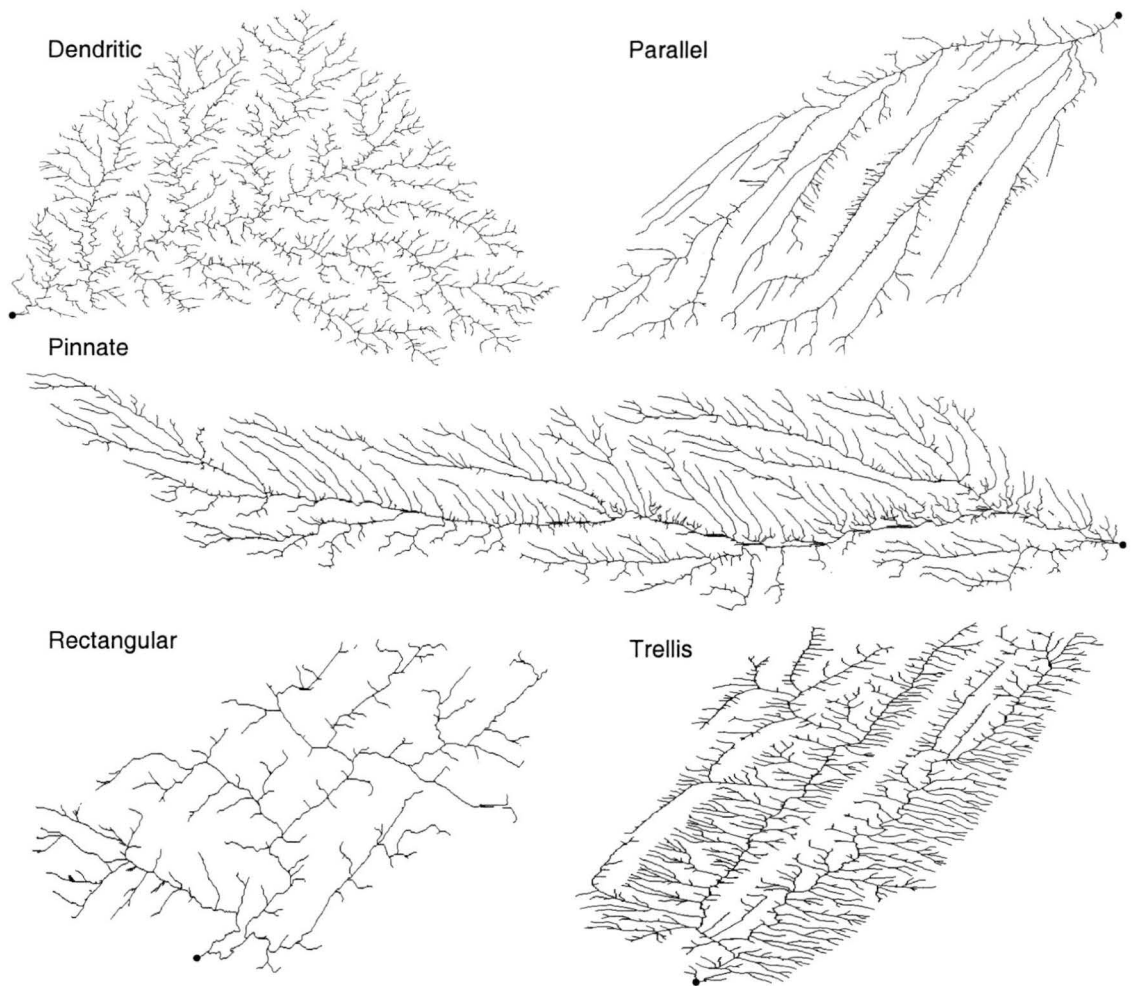


Figure 1.1. Examples of the five network classifications analyzed in this paper. The dots in the figure identify the basin outlets.

2 Planform Self-similarity

Numerous empirical and theoretical results suggest that the planforms of many channel networks are approximately self-similar [Rodríguez-Iturbe *et al.*, 1992; Peckham, 1995; Rigon *et al.*, 1996; Dodds and Rothman, 1999; Veneziano and Niemann, 2000a, 2000b; Niemann and Hasbargen, 2005]. Planform self-similarity means that horizontal properties of a small sub-basin appear statistically identical to the same properties of a large basin if the small sub-basin is isotropically rescaled to appear the same size. This type of self-similarity refers mainly to the channel network and basin boundary, which are properties that can be represented in the horizontal plane. It is understood that this condition applies to a limited range of scales [Montgomery and Dietrich, 1992]. Peckham [1995] considered the topological self-similarity of stream networks using Strahler stream ordering to determine the scales of channels. For streams of order ω , he found that the average number of side tributaries of order $\omega-i$ for a selected i ($i < \omega$) was constant irrespective of the value of ω . This result, which he demonstrated for two large river basins, supports the occurrence of topological self-similarity for dendritic basins. Rigon *et al.* [1996] considered whether the planform geometries of basins are self-similar by examining the behavior of the basin width as the basin length increases. They found that the width increases with length according to a power law with an exponent around 0.93, which suggests that the shapes of basins tend to be approximately self-similar. Furthermore, Rigon *et al.* [1996] and Dodds and Rothman [1999] demonstrated that

many of the power laws observed for natural basins are consistent with channel network self-similarity, fractality or self-affinity of channel courses, and uniform drainage density. It should be noted that in most cases, these authors considered “typical” networks, implying they are not strongly constrained by lithologic or tectonic properties and therefore would be considered dendritic.

Several specific conditions have been proposed to describe the planform self-similarity of networks [Peckham, 1995; Dodds and Rothman, 1999; Veneziano and Niemann, 2000a]. One such condition can be written mathematically as:

$$\zeta(L) \stackrel{d}{=} r^{-D} \zeta(rL), \quad (1)$$

where $\zeta(L)$ is a horizontal property of a network or basin with a linear size L and $\zeta(rL)$ is a horizontal property of a network with linear size rL . r relates the linear sizes of the two networks, and D is the dimension of the network property (e.g., $D = 1$ if ζ is a linear property and $D = 2$ if ζ is an area) [Veneziano and Niemann, 2000b; Niemann and Hasbargen, 2005]. The linear measure of network size can be determined in many ways. In this paper, we use the Euclidean distance between the basin outlet and the mainstream source. The mainstream is identified by starting at the outlet and following the tributary with the larger drainage area at every junction of tributaries. The symbol $\stackrel{d}{=}$ indicates that the left and right sides of the equation are statistically identical. Equation (1) implies that any chosen horizontal property of a basin of size L is drawn from the same distribution as the same horizontal property of a basin of size rL if the latter basin is isotropically rescaled to be the same size. The scaling is isotropic because the scaling exponent depends only on the dimension of the measure ζ , not on the orientation of the property. Because the rescaling is isotropic, the condition implies self-similarity. This

condition differs from traditional self-similarity because it requires one to compare small scale properties of small sub-basins to large scale properties of large basins. Traditional self-similarity allows one to select properties of any sub-region for comparison to any larger sub-region.

This condition of horizontal self-similarity is derived from a more general three-dimensional self-affinity condition for river basin topography in *Veneziano and Niemann* [2000a; 2000b]. Importantly, *Veneziano and Niemann* [2000a] showed that a detachment-limited model [*Howard*, 1994] with an erosion equation based on either shear stress or stream power usually does not destroy this three-dimensional self-affinity if present. *Veneziano and Niemann* [2000b] also demonstrated that this condition is consistent with numerous power-laws that are commonly observed for dendritic networks including the slope-area law [*Hack*, 1957; *Flint*, 1974] and Hack's law [*Hack*, 1957].

It is possible that some other network types exhibit horizontal self-affinity instead of self-similarity. Self-affinity would mean that horizontal properties of a small sub-basin appear statistically identical to the same properties of a large basin if the small sub-basin is anisotropically rescaled to appear the same size. If self-affinity applies, then the scaling exponent in Equation (1) depends on the orientation of the measure being considered. Thus, one must restrict the condition to apply to linear measures and generalize the condition by allowing different scaling exponents for different directions. If we assume that the axis of anisotropy occurs perpendicular to the axis formed by the mainstream source and the basin outlet, then Equation (1) can be written:

$$\zeta_{\parallel}(L) = r^{-d} \zeta_{\parallel}(rL), \quad (2)$$

$$\zeta_{\perp}(L) = r^{-H} \zeta_{\perp}(rL), \quad (3)$$

where $\zeta_{\parallel}(L)$ is a linear property measured parallel to the axis formed by the mainstream source and the outlet, $\zeta_{\perp}(L)$ is a linear property measured perpendicular to $\zeta_{\parallel}(L)$, and H is the self-affinity parameter or Hurst exponent, which describes the degree of anisotropy. If $H = 1$, the anisotropy disappears and the equations imply self-similarity. Although the conditions in Equations (2) and (3) are restricted to apply to linear measures, one can easily derive conditions for areas as well. For example, the area of a basin $A(L) \propto LW(L)$, where $W(L)$ is the width of the basin (measured perpendicular to L). The scaling of L and $W(L)$ are governed by Equations (2) and (3), respectively, so a condition for the area can also be derived. The self-affinity condition could also be generalized to a multifractality condition by replacing H with a carefully selected random variable. This generalization allows more flexibility in explaining the higher moments of the variable across scales, specifically allowing non-linear variation with moment order [Schertzer and Lovejoy, 1987; Gupta and Waymire, 1993; Veneziano and Niemann, 2000a].

2.1 Drainage Area Increments

Ichoku and Chorowicz [1994] observed that the average lengths of channels between junctions (i.e. link lengths) were different for certain network types. For example, they found that parallel networks tend to have very long exterior links. In contrast, pinnate and trellis networks were found to have shorter exterior links and low-order Strahler streams. If a channel has long links or widely-spaced tributary junctions, it also has less frequent increases in its drainage area because area is accumulated primarily where tributaries join. Thus, the first measure we use to characterize the network types is

the incremental accumulation of drainage area along a channel. This measure was previously considered by *Veneziano and Niemann* [2000b], who derived it from the planform self-similarity condition, and *Niemann and Hasbargen* [2005], who used a similar measure to compare experimental and dendritic basin shapes. If the horizontal characteristic in the self-similarity condition (Equation (1)) is chosen to be basin area A , then $D = 2$, and one can write:

$$A(L) = r^{-2} A(rL). \quad (4)$$

If one chooses the length in Equation (4) to be $L - bL$ where b is a constant (which we call the ruler factor), then one can also write:

$$A(L - bL) = r^{-2} A[r(L - bL)]. \quad (5)$$

Taking the difference between Equations (4) and (5) gives:

$$A(L) - A(L - bL) = r^{-2} [A(rL) - A(rL - rbL)]. \quad (6)$$

The left side of the equation is the drainage area increment between points identified by L and $L - bL$. L is the size of the larger basin measured linearly from outlet to the mainstream source and $L - bL$ is the size of the sub-basin or smaller basin measured in the same way. To simplify notation, the left side of the equation can be written $\Delta A_b(L)$ where the term in the parentheses indicates the size of the basin at the downstream point and the subscript indicates the size of the segment over which ΔA is measured. With this notation, Equation (6) can be rewritten:

$$\Delta A_b(L) = r^{-2} \Delta A_{rb}(rL). \quad (7)$$

This relation holds for all L , so one can choose $L = 1$. In that case, r takes on the meaning of L , and the equation can be written:

$$\Delta A_b(1) =^d L^{-2} \Delta A_{bL}(L). \quad (8)$$

The left side of this equation is simply a random variable if b is held fixed. Thus, the right side must have the same probability distribution as the left side for any choice of L . If we plot $\Delta A_{bL}(L)/L^2$ (for a fixed value of b) as we choose points in the basin with different values of L , we should observe a stationary process. Self-similarity requires stationarity in all moments of this process including the mean and the variance, but it does not specify the values of the moments.

Figure 2.1a illustrates the terms used in Equation (8) and the way in which $\Delta A_{bL}(L)$ and L are measured in practice. Each cell in a network of interest is selected as the outlet of a sub-basin, and the sub-basin's area $A(L)$ and Euclidean length L are measured. The drainage area $A(L-bL)$ is obtained by moving a Euclidean distance bL upstream of the point along the mainstream and measuring the area at the new point. The normalized increase in the drainage area over this distance $\Delta A_{bL}(L)/L^2$ can be calculated once $A(L)$, $A(L-bL)$, and L are known. This procedure is repeated for each grid cell in the basin, and the values of $\Delta A_{bL}(L)$ are plotted against L in log-log to evaluate whether self-similarity is observed in the drainage area increments.

If a basin is self-affine, one can use Equations (2) and (3) to obtain a similar condition for the drainage area increments. As noted earlier, the area of a basin is proportional to the Euclidean basin length multiplied by the Euclidean basin width, so one can write:

$$A(L) \propto LW(L). \quad (9)$$

If the characteristic in Equation (2) is chosen to be the basin length and the characteristic in Equation (3) is chosen to be the basin width, then one can write:

$$L(L) = r^{-1} L(rL), \quad (10)$$

$$W(L) = r^{-H} W(rL). \quad (11)$$

Substituting these relationships in for L and $W(L)$ in Equation (9) and noting that $L(rL)W(rL) \propto A(rL)$, one can obtain:

$$A(L) = r^{-1-H} A(rL). \quad (12)$$

This relationship can then be used instead of Equation (4) to derive the following scaling condition for the area increments in a self-affine basin:

$$\Delta A_b(1) = L^{-1-H} \Delta A_{bL}(L). \quad (13)$$

This expression suggests that a plot of $\Delta A_{bL}(L) / L^{1+H}$ against L should be stationary. Because H is not generally known in advance, such a plot is not convenient to develop. Instead, we note that if we plot $\Delta A_{bL}(L) / L^2$ against L and observe a slope, then one can estimate the Hurst exponent as $H = \text{slope} + 1$.

2.2 Stream Course Irregularity

Ichoku and Chorowicz [1994] also observed that the sinuosity of channels varies between different network types. In particular, small channels in parallel and trellis networks tend to be unusually straight, whereas channels in rectangular networks are unusually sinuous. Dendritic self-similarity also has implications for stream course irregularity. This measure was developed by *Veneziano and Niemann* [2000b] and used by *Niemann and Hasbargen* [2005]. Instead of selecting ζ to be the drainage area of a

basin, we choose it to be the standard deviation of the stream course. From Equation (1), one can obtain:

$$\sigma_b(L) = r^{-1} \sigma_{rb}(rL), \quad (14)$$

where we have used $D=1$ because the standard deviation is a linear measure. The subscript on σ indicates the upstream length over which the standard deviation is measured, and the term in the parentheses indicates the linear size of the associated network. The standard deviation is measured in the direction perpendicular to the stream segment under consideration. Following the same procedure that was used for the accumulation of area, one can determine that the distribution of $\sigma_{bL}(L)/L$ (where b is held constant) should be constant irrespective of the choice of L . Again, self-similarity does not constrain the mean or variance of σ ; it only requires that these moments remain constant for all L .

Figure 2.1b illustrates the way that the terms in Equation (14) are measured. The general approach is quite similar to the approach for the drainage area increments. Each cell in the network is selected as the outlet of a sub-basin, and the Euclidean length of the sub-basin L is measured. One then identifies the point that is a Euclidean distance bL upstream from the outlet and measures the standard deviation of the stream course between the two points. Mathematically, the standard deviation is simply:

$$\sigma_{bL}(L) = \frac{1}{n-1} \left[\sum_{i=1}^n (y_i - \bar{y})^2 \right]^{1/2} \quad (15)$$

where n is the number of grid cells available between the two endpoints and y is the offset of each grid cell measured perpendicular to the line connecting the two endpoints. Strictly speaking, n should be held constant for all outlets considered. However, because

the networks will be obtained from DEM data, the available resolution is limited, and n will be determined by the number of available grid cells within the segment being characterized. Once $\sigma_{bL}(L)/L$ is calculated for all locations, it can be plotted against L in log-log to identify potential deviations from self-similarity.

One can derive a similar expression using the self-affinity condition. In this case, one only needs to use Equation (3) because the standard deviation is measured approximately perpendicular to L . If we select $\zeta_{\perp}(L)$ in Equation (3) to be the standard deviation, one can obtain:

$$\sigma_b(L) = r^{-H} \sigma_{rb}(rL). \quad (16)$$

This expression implies that plot of $\sigma_{bL}(L)/L^H$ against L is stationary. More conveniently, it implies that a plot of $\sigma_{bL}(L)/L$ against L has a slope, and $H = \text{slope} + 1$.

2.3 Tributary Junction Angles

Abrahams and Flint [1983], *Phillips and Schumm* [1987], and *Ichoku and Chorowicz* [1994] all observed differences in the tributary junction angles for different network types. In particular, parallel networks seem to have an abundance of very small junction angles, whereas rectangular and trellis networks seem to have an abundance of right and obtuse junction angles, respectively. Although it has not been considered previously, planform self-similarity also applies to the angles at which tributaries join the mainstream. In this case, ζ is selected to be the angle formed between the primary tributary and the secondary tributary at a junction, which we denote by ψ . By primary

tributary, we mean the extension of the mainstream upstream from the junction. In this case, self-similarity implies:

$$\psi_{b,b}(L) \stackrel{d}{=} \psi_{rb,rb}(rL), \quad (17)$$

where the subscripts on ψ indicates the chord lengths that are used on the primary and secondary tributaries to measure the junction angle. If L is chosen to be one, then r takes on the meaning of L and:

$$\psi_{b,b}(1) \stackrel{d}{=} \psi_{bL,bL}(L), \quad (18)$$

where the left side is simply a random variable, which suggests that the $\psi_{bL,bL}(L)$ has the same distribution irrespective of L . For a self-similar network, the distribution of secondary tributary sizes is expected to scale with L . This means we can also measure the junction angle using a chord length of bL on the primary tributary and bL_i on the secondary tributary, where L_i is the Euclidean length of the secondary tributary's basin. In this case, the measured angle is denoted $\psi_{bL,bL_i}(L)$. Figure 2.1c illustrates the measurement of $\psi_{bL,bL_i}(L)$. Each point in the network is considered as a possible junction location. If a junction is present, then the junction angle is measured. The chord length used to measure the orientation of the primary tributary is bL , and the chord length used to measure the orientation of the secondary tributary is bL_i . Notice if b is near zero, the junction angle is measured more locally, and if b is near one, the junction angle is measured using the entire lengths of the tributary basins.

It has been suggested by numerous authors that junction angles (at least in dendritic basins) depend on the ratio of the two tributary sizes. *Lubowe* [1964] showed that the junction angle increases as the ratio of the two tributary orders increases, and

Pieri [1984] found the junction angle increases as the ratio of the tributary magnitudes increases. Similarly, *Horton* [1932] suggested that the tributary angle tends to increase as the ratio of the two tributary slopes increases, and several studies have found this to be true for natural networks (e.g., *Schumm* [1956], *Lubowe* [1964], and *Howard* [1971]). *Horton's* model is consistent with the other results because channel slope generally varies with drainage area [*Hack*, 1957; *Flint*, 1974].

These empirical results are compatible with an infinite self-similar network because the distribution of the ratio of tributary sizes is expected to remain constant throughout the network. For networks that are finite in size, however, the distribution is expected to change with L . When L is large, a wide range of tributaries sizes are possible, but when L is small, only tributaries that are relatively large in comparison to L are possible. This tendency might impact a plot of $\psi_{bL,bl_t}(L)$ against L . To evaluate self-similarity under these circumstances, one could consider only junctions where the secondary tributary falls within a range of sizes that is specified relative L . Specifically, one can consider tributaries with $c_1L < L_t < c_2L$ where c_1 and c_2 are constants (both must be between 0 and 1).

It is important to note that the methodology described above cannot be directly generalized for the case of self-affinity. If self-affinity applies, then the appropriate chord length for the secondary tributary depends on the junction angle itself. If the angle is 90° , this chord length should scale according to L^H , if it is 0° , then it should scale with L . Thus, one cannot use plots of the junction angles against L to infer self-affinity or a value of H .

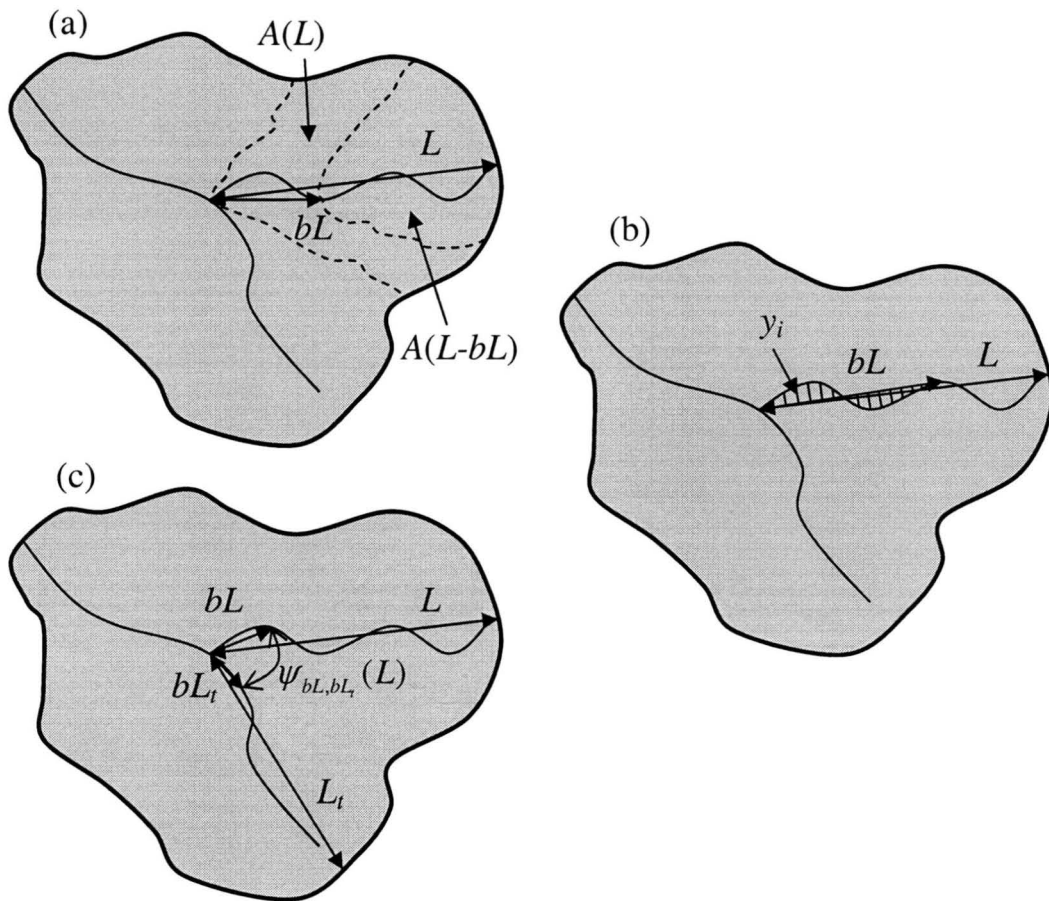


Figure 2.1. Illustration of the measurement of (a) the drainage area increments, (b) the stream course irregularity, and (c) the junction angles.

3 Dataset

Ten networks were identified for each network classification as shown in Table 1. These networks were selected because they were explicitly classified previously or they are located in regions where a certain network type is known to predominate. Where possible, basins were selected from regions with higher resolution DEM data. The dendritic basins were previously classified by *Zernitz* [1932] and *Lubowe* [1964]. *Zernitz* [1932] identified the Allegheny Plateau in West Virginia and the southern part of the Atlantic coastal plains in Georgia and South Carolina as regions where dendritic networks commonly occur. *Lubowe* [1964] and *De Serres and Roy* [1990] also identified dendritic drainages in sections of the Appalachian Plateau and the interior low plateaus in Kentucky that are underlain by sedimentary rock and horizontal strata. The parallel networks were previously classified by *Zernitz* [1932] and *Phillips and Schumm* [1987]. *Zernitz* [1932] identified several locations in Utah where parallel networks can be observed, and *Phillips and Schumm* [1987] characterized parallel networks in several areas in Colorado and Wyoming. Pinnate networks were selected mainly based on the observations of *Zernitz* [1932]. From visual inspection, *Zernitz* [1932] identified pinnate networks in portions of Romania (now Moldova and Ukraine). The selected pinnate networks are tributaries to the Dniester River in western Ukraine and tributaries to the Nistru River in eastern Moldova. The rectangular networks were originally classified by *Zernitz* [1932]. They are all from northern New York in the vicinity of Elizabethtown.

The trellis networks are all from the ridge and valley sections of the Appalachians in Maryland, Pennsylvania, Tennessee, Virginia, and West Virginia. The drainage networks of this region were classified as trellis by *Zernitz* [1932], *Mock* [1971], and *Abrahams and Flint* [1983].

For each of the selected basins, DEM data were obtained through the Seamless Data Distribution System (SDDS) from the United States Geological Survey. For basins within the United States, the National Elevation Dataset (NED) was used to obtain data in raster format with resolution of 1 arc second (approximately 30 meter grid cells). For the rest of the globe, the finished dataset from the Shuttle Radar Topography Mission (SRTM) was used to obtain data with resolution of 3 arc seconds (approximately 90 meter grid cells). For simplicity, the grid cell size was assumed to be constant within each basin considered. The cell size for each basin was determined by computing an average grid cell dimension using the extreme north, south, east, and west boundaries of the basin [*Maling*, 1992; *Van Sickle*, 2004]. After filling pits, flow directions were computed by examining the eight surrounding cells and determining the direction of steepest descent [*O'Callaghan and Mark*, 1984; *Tarboton et al.*, 1991]. From the flow directions, the drainage areas were computed by summing the total areas draining through each grid cell [*O'Callaghan and Mark*, 1984; *Tarboton et al.*, 1991].

Because our analysis considers only the channel network, a method is required to identify the channel network from the DEM topography. Three general methods have been proposed to determine the initiation of channels. *Horton* [1932; 1945] initially suggested that channels begin after a threshold in hillslope length is surpassed. More recently, *Tarboton et al.* [1991] suggested the use of a threshold drainage area. Grid cells

are assumed to contain a channel if their drainage area exceeds a specified threshold. *Montgomery and Foufoula-Georgiou* [1993] suggested the use of a threshold shear stress, where shear stress is calculated as a function of both drainage area and slope. For the purposes of our analysis, the drainage density does not need to be estimated very accurately. It is more important to conservatively estimate the extent of the channel network so that the analyzed channels are larger with respect to the DEM resolution. Furthermore, the approach should not introduce biases in the consideration of scaling invariance. Given these criteria, the best method is to use a length threshold because we use basin length as our linear measure of basin size (Section 2). If a threshold area is used to identify the extent of channelization, it implicitly places a constraint on the basin shapes that are allowed for small basin lengths. Similar problems would arise if a threshold shear stress were used. Because length is likely the least reliable method for estimating the extent of the channel network, this approach should be regarded as a pruning of the channel network rather than an estimation of the actual extent of the drainage network.

The value of the length threshold was identified using the slope-area plot (i.e. a log-log plot of the channel slopes against the associated drainage areas). In this plot, a reversal point is usually observed where the relationship between the average slope and drainage area changes from positive to negative. *Montgomery and Foufoula-Georgiou* [1993] suggested the use of this point to distinguish the hillslopes and channels. This area is divided by the smallest grid cell dimension to determine an associated length threshold. This length is the longest possible hillslope that can occur for the area threshold. If this length threshold is used, the network typically exhibits a feathered

appearance where adjacent parallel channels are observed near the channel heads. The feathering likely occurs because the channelization has become finer than the resolution of DEM, but it may also suggest the occurrence of planar or divergent hillslopes. Either way, such points should be excluded from the analysis. The length threshold was increased until the feathering disappeared. When the feathering disappears, the resulting network is used for analysis. The example networks shown in Figure 1 were obtained following the procedure outlined above.

Table 3.1. Basins analyzed including the author who previously classified the basin.

Network Type	Stream Name	Outlet Lat. and Long. (Deg.)	Area (km ²)
Dendritic	Bluestone Creek, WV*	39.302083, -80.778750	324
	Buckeye Run, WV*	29.319860, -80.806528	318
	Buffalo Creek, WV*	40.250973, -80.597639	419
	Captina Creek, OH*	39.870694, -80.819306	460
	Cedar Creek, AL*	31.671251, -81.504861	219
	Little Saluda River, SC*	34.077362, -81.594028	565
	Tenmile Creek, PA-	39.980418, -80.024028	512
	Turkey Creek, SC*	33.777363, -82.160694	550
	Tygarts Creek, KY-	38.392639, -82.960139	291
	Wheeling Creek, WV*	40.050696, -80.667361	739
Parallel	Albert Creek, WY+	41.506527, -110.60958	438
	Black Sulphur Creek, CO+	39.867639, -108.29319	266
	Duck Creek, CO+	39.978750, -108.38208	142
	Greasewood Creek, CO+	40.130139, -108.41264	61
	Hill Creek, UT*	39.665140, -109.730690	388
	Picceance River, Trib. 1, CO+	39.888472, -108.39597	74
	Picceance River, Trib. 2, CO+	39.862094, -108.299860	259
	Sheep Creek, WY+	41.564583, -110.61542	487
	Willow Creek, UT*	39.422363, -109.629310	350
	Yellow Creek, CO+	39.965417, -108.38986	85
Pinnate	Dniester River Trib. 1, Ukraine*	47.914581, 30.636250	2114
	Dniester River Trib. 2, Ukraine*	48.124581, 30.006250	1356
	Dniester River Trib. 3, Ukraine*	46.354579, 28.941250	1005
	Dniester River Trib. 4, Ukraine*	46.793749, 29.980417	1573
	Dniester River Trib. 5, Ukraine*	46.614582, 29.284583	1084
	Dniester River Trib. 6, Ukraine*	47.139580, 28.906250	761
	Nistru River Trib. 1, Moldova*	47.379580, 30.506250	697
	Nistru River Trib. 2, Moldova*	47.389580, 30.556250	589
	Nistru River Trib. 4, Moldova*	46.111249, 28.612917	723
	Nistru River Trib. 5, Moldova*	46.052916, 28.758750	350
Rectangular	Boquet River, NY*	44.242360, -73.462083	239
	Boreas River, NY*	43.832085, -74.070972	218
	Cold River, NY*	44.103751, -74.312639	218
	Hudson River, NY*	43.968193, -74.052639	198
	Saint Regis River, NY*	44.532083, -74.472361	344
	Salmon River, NY*	44.867361, -74.297083	475
	Schroon River, NY*	43.955693, -73.733750	239
	Summer Brook, NY*	44.407638, -74.083750	147
	Walker Brook, NY*	44.000416, -73.712639	133
	West Branch St Regis River, NY*	44.438749, -74.591250	304
Trellis	Aughwick Creek, PA/	40.298750, -77.887361	823
	Cacapon River, WV*	39.253356, -78.454931	477
	Evitts Creek, MD*	39.664028, -78.732083	240
	Jackson River, VA*	39.165140, -79.750972	251
	Juniata River, PA/	40.507083, -77.438194	530
	Lick Branch, TN*	35.245140, -84.656528	339
	Middle Creek, PA*	40.764306, -76.884583	219
	Peters Run, WV*	38.722917, -79.304306	609
	Sleepy Creek, WV*	39.620694, -78.145972	294
	Stony Run, WV*	38.745140, -79.287639	828

* Zernitz [1932] - Lubowe [1965] + Phillips and Schumm [1987] / Abrahams and Flint [1983]

4 Results

4.1 Selection of Ruler Factor

One very important step in the calculation of the drainage network properties is the selection of an appropriate ruler factor b . Figure 4.1 considers how the choice of b affects the results of the three measures. To generate this figure, the three properties were calculated for all possible sub-basins in a dendritic network (Turkey Creek). The average value of each property was then calculated for small ranges of basin length. In Figure 4.1, these averages are plotted as a function of basin length. This process was repeated for each measure using three values of b . In Figure 4.1a and 4.1b, the same set of b values are used for both the drainage area increments and the stream course irregularity. For the junction angles in Figure 4.1c, smaller values of b are used in order to measure the angles using chords that remain relatively close to the junction.

Figure 4.1 demonstrates two important limitations that constrain the choice of b . First, as one chooses larger values of b , one restricts the range of basin sizes that can be evaluated. This is particularly evident in Figures 3a and 3b where the values of b are relatively large. As b becomes large, the properties are measured over longer channel segments for a given sub-basin size. As the segment length increases, there is a greater likelihood that the upstream end of the segment will encounter a hillslope grid cell and thus be removed from consideration. Second, as one chooses smaller values of b , one tends to observe deviations from a horizontal line for small basin lengths. This tendency

is particularly evident in Figures 3b and 3c. As b becomes small, one measures the properties over shorter channel segments. For small basin lengths, these segments might include only a few grid cells, so the grid resolution has a strong impact on the measures. For the analyses that follow, we want to consider the largest number of sub-basin sizes possible without encountering significant biases due to the grid resolution. Based on Figure 4.1 and similar plots from other basins, we selected $b = 0.2$ for the drainage area increments, $b = 0.4$ for stream course irregularity, and $b = 0.1$ for the junction angles. It should also be noted from Figure 4.1 that the average values of the drainage area increment and stream course irregularity are sensitive to the choice of b . In both cases, these properties increase as one considers longer stream segments. The junction angles remain relatively constant over the range of b values considered (the junction angle lines have been offset in Figure 4.1 for clarity).

4.2 Dendritic Networks

In this section, we apply the three measures to dendritic basins. Our objectives are to confirm that self-similarity applies to dendritic basins and (if it does) to use the normalized properties from each of the measures to characterize dendritic basins. The three measures were applied to the 10 dendritic basins, and Figure 4.2 shows the results for 4 typical basins. Figure 4.2 was generated in the same manner as Figure 4.1, but uses only one value of b for each measure. As discussed in Section 2, all of the normalized measures should produce horizontal lines if self-similarity applies. Overall, the plots in Figure 4.2 are close to horizontal although some fluctuations are observed at large basin scales. These fluctuations occur because fewer channels are available to calculate the

average measures for large basin lengths. To assess the significance of the observed slopes, regression lines were fitted to the plots in log-log and are shown by the dashed lines. Furthermore, T tests were performed to test the null hypothesis that the slope of the regression line is zero at the 95% confidence level. If the null hypothesis is rejected, the slope is considered significant. It should be noted that the T test relies on the assumptions that the errors are independent, normally distributed, and have homogenous variance. Because the regression was performed on average drainage area increment values, which are calculated from non-overlapping bins of basin length, the first two assumptions are reasonable. However, the number of observations used to calculate the average changes with basin length, so the error variance is expected to be heterogeneous. Thus, the T test results provide informative but inexact evaluations of the significance of the slopes. For the drainage area increments, the average slope estimate from all 10 basins is -0.007, and the range of slopes is -0.079 to 0.041. In all cases, the slope is small, and the T test confirms that none of the slopes is statistically different from zero at the 95% confidence level. For the stream course irregularity, the average slope from all the basins is 0.0303 with a range from -0.028 to 0.080. Again, none of these slopes are considered significant by the T test. Finally, the average slope of the junction angle plots is -2.95 with a range from -11.28 to 7.25. The slope is considered significant for 3 of the 10 basins at the 95% confidence level. Overall, the results support the hypothesis that dendritic basins are self-similar.

Given the stability of the normalized measures across a range of basin sizes, it is also worth examining the values of these measures to characterize dendritic basins. To this purpose, we estimated the average value for the drainage area increments to be 0.147

among the 10 dendritic basins. Because this value was determined with $b = 0.2$, loosely speaking, it means that a 14.7% increase in drainage area typically occurs in the lower 20% of a basin's length. This value ranges from 0.139 to 0.157 for the individual basins, which is only 12% of the average calculated from all ten basins. This small range suggests that the area accumulation process is similar for all of the dendritic basins that were analyzed. The average for the stream course irregularity is 0.0151, with values ranging from 0.0135 to 0.0164 for the ten basins analyzed. The range in this case is 19% of the average, which suggests that this measure is also relatively constant between the dendritic basins analyzed. The average tributary junction angle is 65.5 degrees (the range is 57.8 to 71.4 degrees, which is 21% of the average). These results are consistent with values found in the literature. For example, *Lubowe* [1964] found that the average junction angles ranged from 60 to 80 degrees among 4 different dendritic basins, and *Ichoku and Chorowicz* [1994] also found that the average angle is close to 60 degrees. In both cases, the junction angles were measured with different chord lengths than those used here.

4.3 Parallel Networks

We now turn our attention to parallel networks to determine whether they exhibit deviations from dendritic self-similarity. The three measures were applied to the 10 parallel networks, and the results for four typical networks are shown in Figure 4.3. The figure shows that negative slopes are usually observed for both the drainage area increments and for the stream course irregularity. For the area increments, the average value of the slope is -0.188, and the range is -0.325 to -0.062. Using the T test, these

slopes are considered significantly different from zero for 8 of the 10 basins. The negative slopes imply that larger basins accumulate less drainage area relative to their size than small basins or equivalently that large basins are more elongated. Referring back to Section 2, it also suggests that the basins may be self-affine. The Hurst exponent H can be estimated from the slope of the drainage area increment plots as $H = \text{slope} + 1$, so from the slopes estimate $H = 0.81$ on average, with a range of estimates from 0.68 to 0.94. Similar behavior is observed for the stream course irregularity. The average slope for this measure is -0.16 (the range is -0.356 to -0.020) and the slopes are statistically different from 0 for 8 of the 10 basins. The negative slopes for this measure indicate that the sinuosity is decreasing with respect to the basin size as the basin size increases. The average slope implies that $H = 0.84$ (the range is 0.64 to 0.98), which is consistent with the H from the drainage area increments.

It should be noted that these results are also consistent with multifractality. The usual method to evaluate whether self-affinity or multifractality occurs is to examine the scaling behavior of different moments of the variable. If the exponents increase linearly with the moment order considered, then self-affinity occurs. If they increase nonlinearly, then multifractality occurs. We plotted the first four initial moments for the stream course irregularity and found a strongly linear behavior with moment order, which confirms that self-affinity occurs.

The junction angle measure typically has a positive slope, which suggests that the average tributary junction angle increases as one moves downstream. The average slope for this measure is 10.9 (the range is 0.7 to 18.2). This result is counter-intuitive because one expects more acute junction angles if basin shapes are becoming more elongated.

However, most tributaries are small relative to the main channel, especially at large basin sizes, and these tributary junction angles may not reflect the elongation. To test this interpretation, Figure 4.4 plots the average junction angles for one dendritic basin and one parallel basin when the included tributaries are restricted to the range $0.6L < L_i < 1.0L$. When the range of tributary sizes is restricted, the average angle for the dendritic network increases slightly from 71.1 to 73.6 degrees. For the parallel network, however, the average angle decreases considerably from 65.6 to 49.9 degrees. Thus, the junction angles formed by large tributaries decrease as expected from visual inspection, but this decrease is masked in the measure by the large number of small tributaries with larger angles.

4.4 Pinnate Networks

The three measures were also applied to the set of 10 pinnate networks, and the results for 4 typical networks are shown in Figure 4.5. Like parallel networks, the drainage area increments and the stream course irregularity exhibit negative slopes. For the area increments, the average slope among the 10 basins is -0.283, and the range of slopes is -0.394 to -0.133. The slopes are considered significant for all 10 basins by the *T* test. These slopes are typically more negative than the slopes for parallel networks, which suggests that more significant self-affinity may occur in the pinnate case. The average slope implies $H = 0.72$, and the range of slopes corresponds to a range of H from 0.61 to 0.87. Similar behavior is observed for the stream course irregularity. The slope is negative (average is -0.308, range is -0.514 to -0.117) and significant for all basins. The average slope implies $H = 0.69$ with a range of H estimates from 0.49 to

0.88. Here again, we see close agreement in the H estimates obtained from the area increments and the stream course irregularity, which supports the contention that a single H applies to both network characteristics. Note that the higher moments of the stream course irregularity were examined and found to vary linearly with moment order, which confirms that the scaling is self-affine.

One important difference from parallel networks is the slope of the tributary junction angle measure. For pinnate networks, the average junction angle tends to decrease with increasing Euclidean basin length. Specifically, we find an average slope for the junction angle measure of -8.11 (the range is -0.68 to -17.26). The negative slope is expected because larger basins tend to be more elongated. The difference in the junction angles of parallel and pinnate networks can also be confirmed by a visual inspection in Figure 1. For the parallel network, small tributaries tend to join the major channels with nearly orthogonal junction angles, whereas larger tributaries have more acute junction angles. For the pinnate network, all tributary sizes seem to have acute junction angles.

4.5 Rectangular Networks

The three measures were also applied to characterize the 10 rectangular networks, and Figure 4.6 shows the results for 4 of these networks. In this case, most of the plots are approximately horizontal, although relatively large fluctuations are observed. For the drainage area increments, the average slope is -0.0462, and the range of slopes is -0.272 to 0.451. The slope is considered significant for only 3 of the 10 basins. For the stream course irregularity, the average slope is 0.0472, and the range is -0.0192 to 0.1622. The

slope is considered significant for only 1 of the 10 basins. For the junction angles, the average slope is 16.68, and the range is 10.79 to 34.39. The slope is considered significant in 2 of the 10 basins. One can see from Figure 4.6 that the non-zero slopes are usually produced by deviations that occur at various basin sizes. The importance of these deviations can be evaluated by calculating the variance of the residuals, which is also the mean square error of the regression line. For the area increments, the average variance of the residuals is 0.0289 compared with 0.0114 for the dendritic networks. For the stream course irregularity, the average residual is 0.0127 compared to 0.0066, and for the junction angles, the average is 12.11 compared to 7.47. Overall, these results suggest that rectangular basins are approximately self-similar, but that significant deviations occur in all three measures at various scales.

If these networks are considered self-similar, then the average values of the measures can be compared to those of dendritic networks. The average of the drainage area increment is 0.138 with a range from 0.111 to 0.171. This range overlaps with the one for dendritic basins but is slightly smaller. The average of the stream course irregularity is 0.0194, and the range is 0.0184 to 0.0217. These values are notably larger than those observed for dendritic basins. In fact, the ranges for these two network types do not overlap. This result suggests that every rectangular network that we analyzed has more irregular stream courses than any dendritic network we analyzed. The average junction angle is 66.0 degrees, and the range is 58.8 to 74.0. Both the average and the range are very similar to the values found for dendritic networks, which suggests that rectangular networks exhibit no abundance of right junction angles using this measure. This result seems to hold even if the range of allowable tributary sizes is decreased.

Anomalous junction angles are observed, but they are generally overwhelmed by the number of acute junction angles.

4.6 Trellis Networks

Ten trellis networks were also analyzed, and the results for 4 of these networks are shown in Figure 4.7. Similar to the rectangular networks, the lines are approximately horizontal, but significant deviations are observed. Interestingly, these deviations tend to occur over wider ranges of basin sizes than the deviations observed for rectangular basins. This tendency makes sense because the ridges that ultimately produce these deviations tend to persist for longer distances than the lineate features visible in rectangular networks (see Figure 1, for example). The average slope of the area increment measures is -0.142, with a range from -0.288 to 0.075. The slope is judged to be significant for 4 of the 10 basins, although the variance of the residuals is 0.0236, which is almost twice that of dendritic basins. For the stream course irregularity, the average slope is -0.084, and the range is -0.2440 to 0.0447. The slope is significantly different from zero in 3 of the 10 basins. The variance of the residuals is 0.0195 compared to 0.0066 for dendritic networks. For the junction angles, the average slope is 10.6, and the range is 1.5 to 21.5. The slope is considered insignificant for the 10 networks. The variance of the residuals is 9.1 compared to 7.5 for dendritic. In the end, the slopes of most of the lines are not considered significantly different from zero, so trellis basins appear to be self-similar, at least in approximation. It is possible that some degree of self-affinity is present, but this self-affinity would require a much larger dataset to reliably quantify.

The average values of the measures can be used to distinguish these basins from dendritic basins. More importantly, the average of the drainage area increment measure is 0.111 and the range is 0.087 to 0.131. This range is lower than and does not overlap with the range for dendritic basins. This suggests that the rate of drainage area accumulation is significantly reduced for trellis networks in comparison to unconstrained networks. For the stream course irregularity measure, the average is 0.0153, with a range of values from 0.0130 to 0.0166. These values are slightly larger than those of dendritic networks. This result is expected. Although the channels in trellis networks tend to have low sinuosity between junctions, they also tend to join at less acute junction angles, which increases the overall irregularity of the courses. The average junction angle in trellis networks is 67.6 degrees, with a range of 60.6 to 77.0 degrees between different networks. The average is a little larger than dendritic, but the ranges overlap. Analogous results were determined by *Ichoku and Chorowicz* [1994]. They found trellis networks always had average angles greater than 60 degrees.

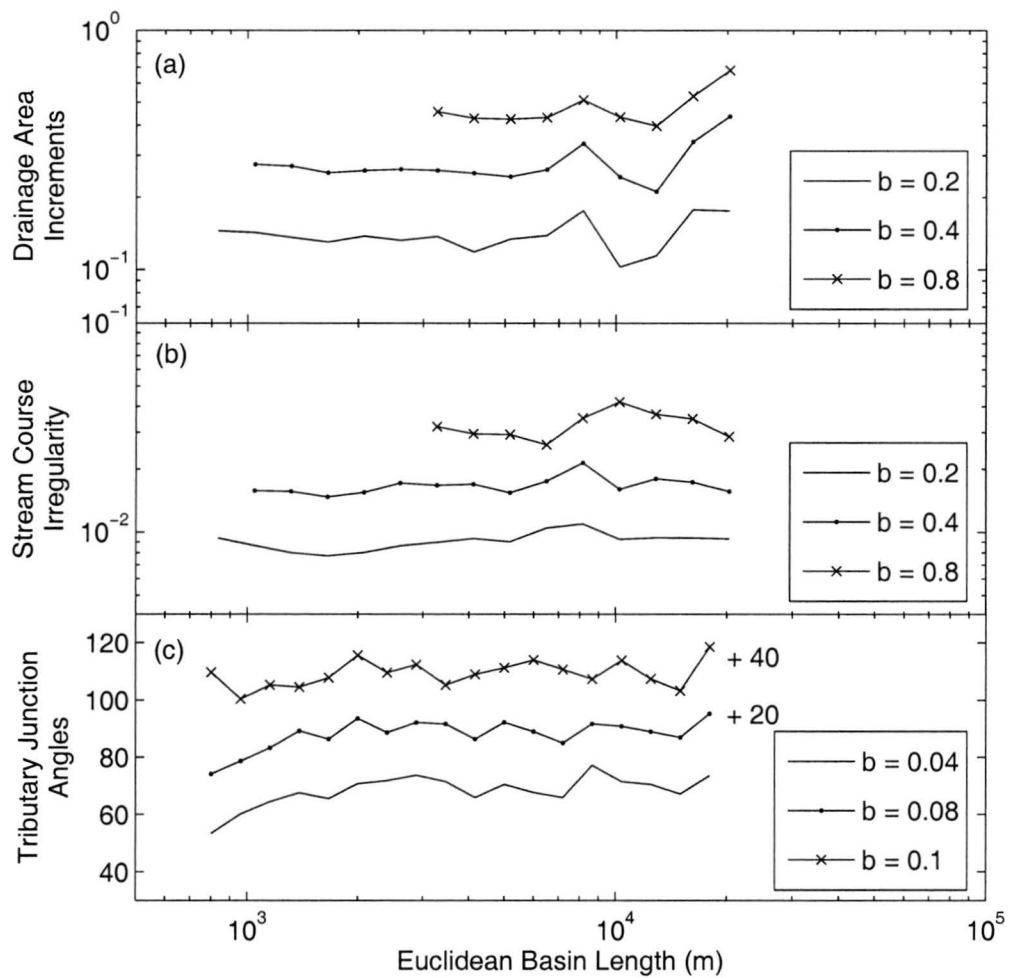


Figure 4.1. Plots of the average values of (a) $\Delta A_{bL}(L)/L^2$, (b) $\sigma_{bL}(L)/L$, and (c) $\psi_{bL,bL_i}(L)$ as a function of basin size L when different values of b are used on a dendritic network (Turkey Creek). The lines in (c) have been offset as indicated in the figure for clarity.

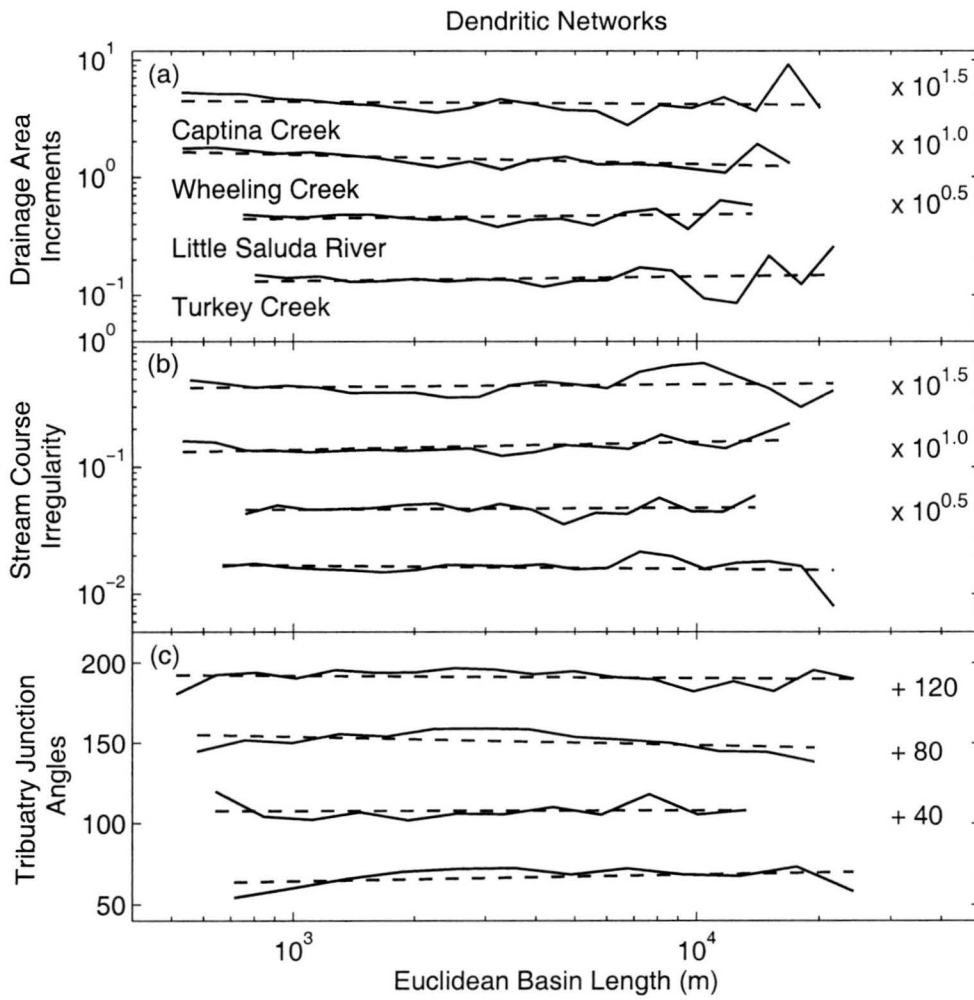


Figure 4.2. Plots of the average values of (a) $\Delta A_{bL}(L)/L^2$, (b) $\sigma_{bL}(L)/L$, and (c) $\psi_{bL,bL_s}(L)$ as a function of basin size L for four typical dendritic networks. The dashed lines show the regression lines fit to the plots of the average values. The lines for the different basins have been offset as indicated in the figure for clarity.

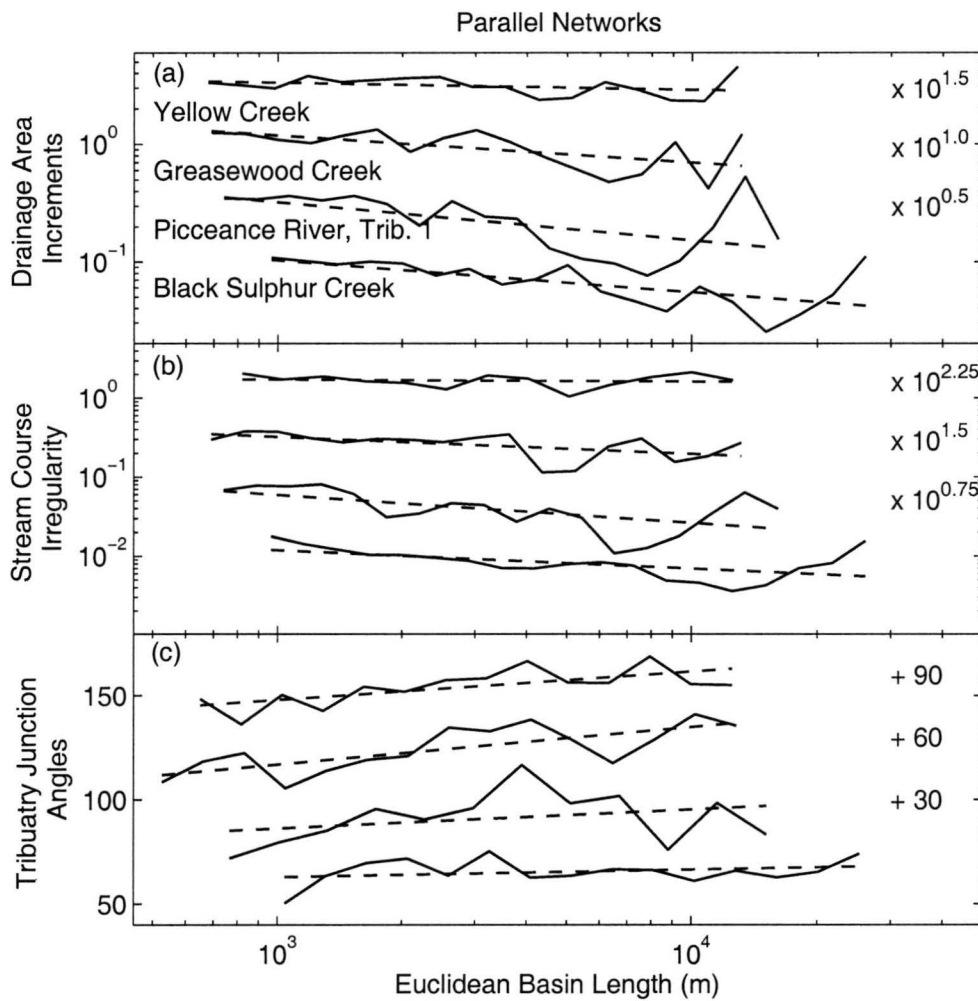


Figure 4.3. Plots of the average values of (a) $\Delta A_{bL}(L)/L^2$, (b) $\sigma_{bL}(L)/L$, and (c) $\psi_{bL,bL}(L)$ as a function of basin size L for four typical parallel networks. The dashed lines show the regression lines fit to the plots of the average values. The lines for the different basins have been offset as indicated in the figure for clarity.

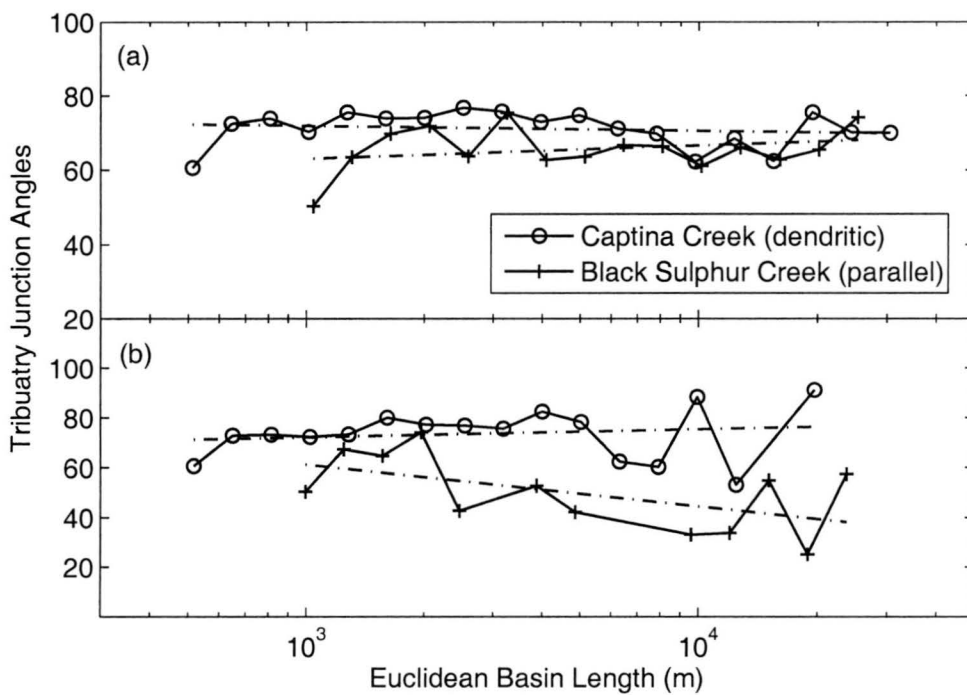


Figure 4.4. Impact of restricting range of tributary sizes used to calculate $\psi_{bL,bL_t}(L)$. In (a), the allowable range of secondary tributary sizes is $0 < L_t < L$. In (b), the allowable range is $0.6L < L_t < 1.0L$.

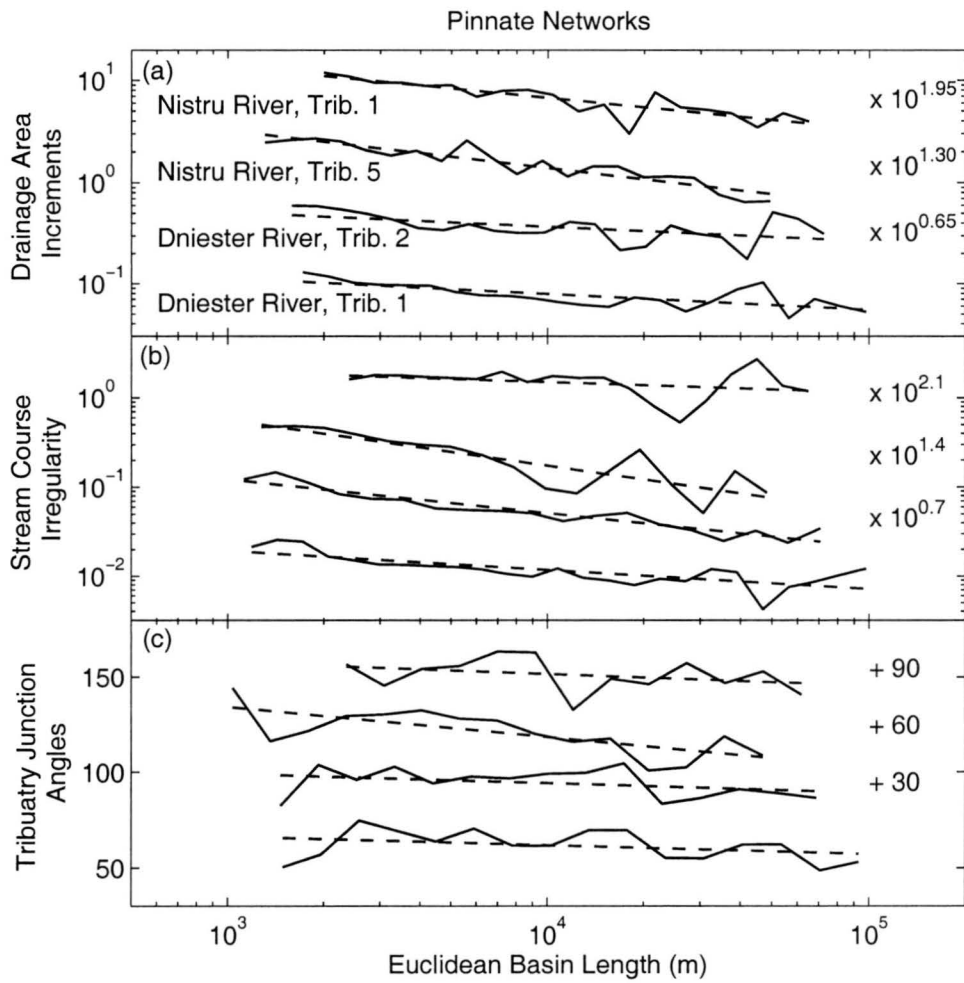


Figure 4.5. Plots of the average values of (a) $\Delta A_{bL}(L)/L^2$, (b) $\sigma_{bL}(L)/L$, and (c) $\psi_{bL,bL_t}(L)$ as a function of basin size L for four typical pinnate networks. The dashed lines show the regression lines fit to the plots of the average values. The lines for the different basins have been offset as indicated in the figure for clarity.

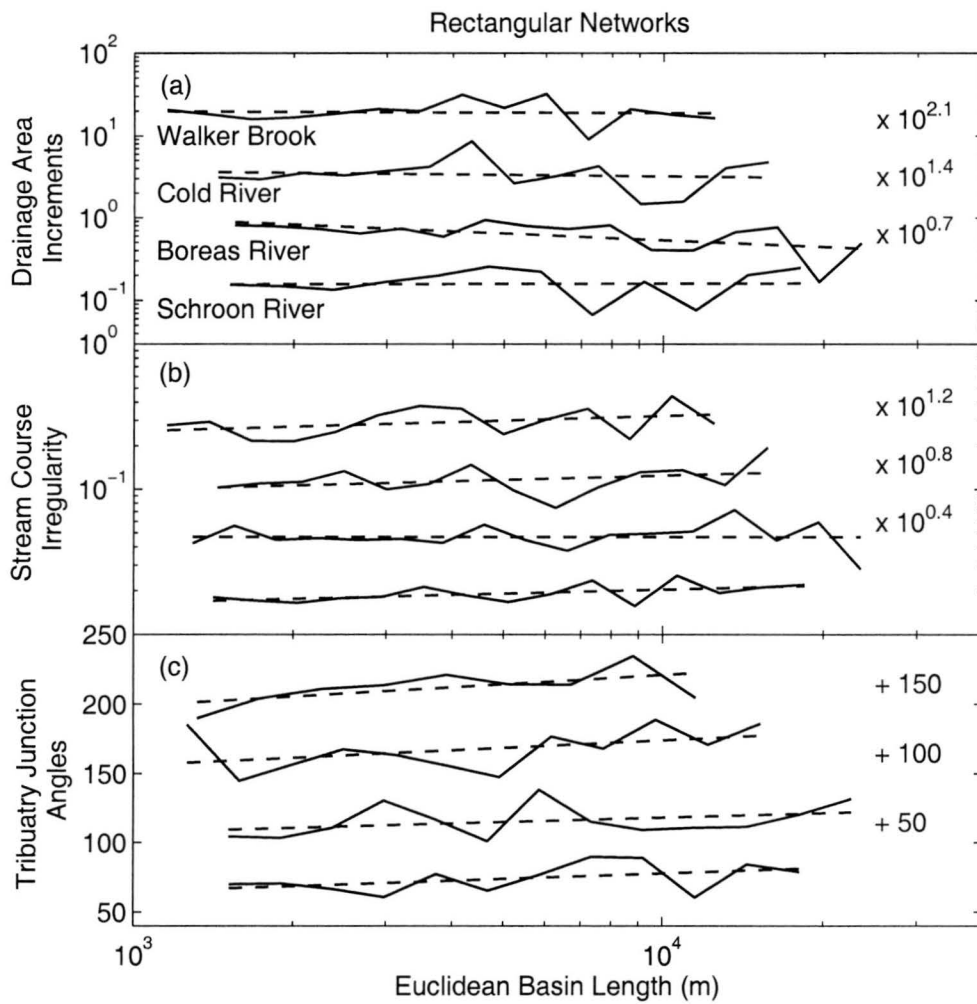


Figure 4.6. Plots of the average values of (a) $\Delta A_{bL}(L)/L^2$, (b) $\sigma_{bL}(L)/L$, and (c) $\psi_{bL,bL_t}(L)$ as a function of basin size L for four typical rectangular networks. The dashed lines show the regression lines fit to the plots of the average values. The lines for the different basins have been offset as indicated in the figure for clarity.

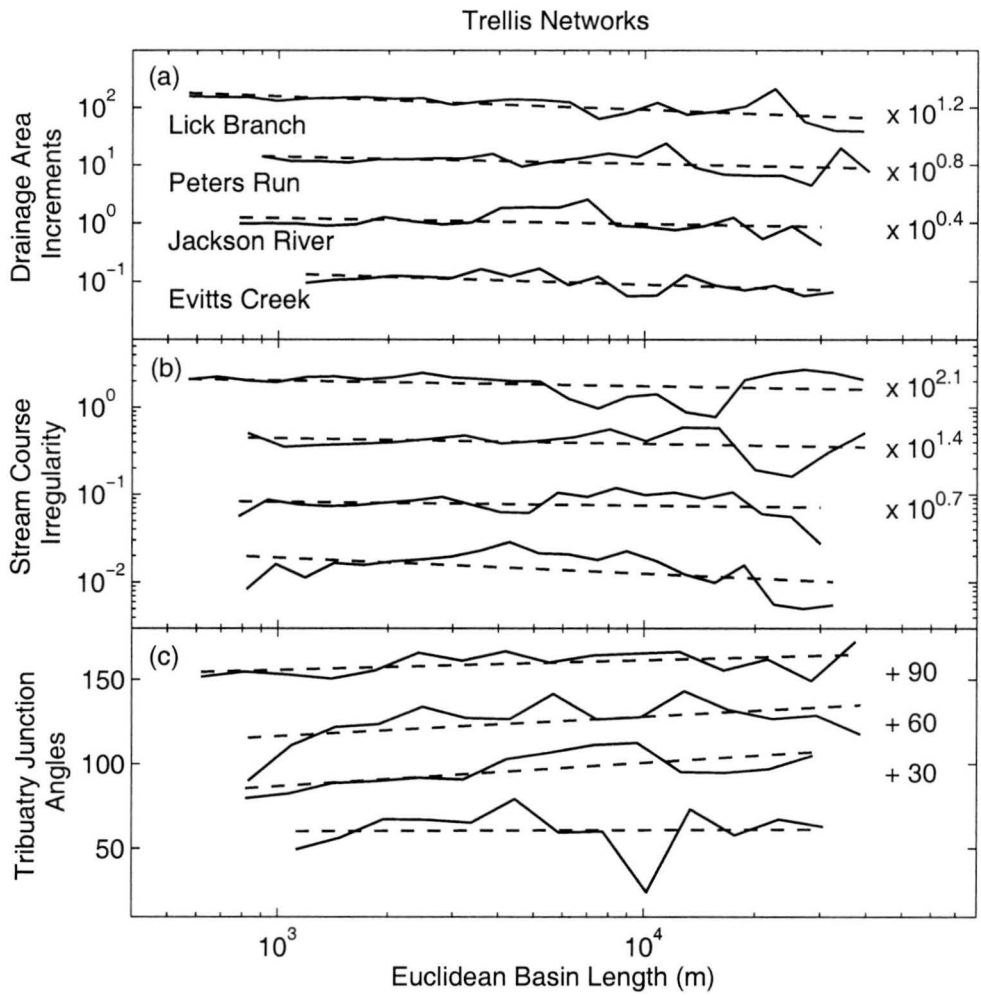


Figure 4.7. Plots of the average values of (a) $\Delta A_{bL}(L)/L^2$, (b) $\sigma_{bL}(L)/L$, and (c) $\psi_{bL,bL_t}(L)$ as a function of basin size L for four typical trellis networks. The dashed lines show the regression lines fit to the plots of the average values. The lines for the different basins have been offset as indicated in the figure for clarity.

5 Classification Method

In this section, the results from Section 4 are used to develop and test a classification method for drainage networks. Various methods can be used for classification such as principal component analysis, artificial neural networks, support vector machines, cluster analysis, and classification trees [White, 1997; Jaynes *et al.*, 2003; Muñoz and Felicísimo, 2004]. A classification tree technique was selected because it is hierarchical, which is consistent with the traditional view of drainage network classifications [Zernitz, 1932; Parvis, 1950; Howard, 1967] as well as previous quantitative classification methods [Ichoku and Chorowicz, 1994]. The results of classification trees are also relatively simple to interpret, and classification trees can handle non-linear and high-dimensional classification problems [Vayssieres *et al.*, 2000]. This technique has been applied in many disciplines [Balk and Elder, 2000; De'ath and Fabricius, 2000; Vayssieres *et al.*, 2000; Gómez-Chova *et al.*, 2003; Bittencourt and Clarke, 2004].

To develop the classification tree for drainage networks, one must first specify the classifications to be considered (dendritic, parallel, pinnate, rectangular, and trellis) and the variables that can be used to distinguish these classifications. The variables we use are the averages, slopes, and residual variances from the regression lines for each of the three measures (shown for all networks in Figures 10, 11, and 12). The entire dataset for

the classification problem consists of 5 classifications, 9 variables, and 50 networks (10 networks for each classification).

The development of the classification tree begins by dividing the dataset of 50 networks into two groups using a set of thresholds for the supplied variables. In our case, we require the method to use a threshold on a single variable in order to simplify the interpretation of the tree. The threshold that achieves the maximum reduction in the “impurity” of the dataset is selected. Mathematically, the method aims to maximize $\Delta i(s, t)$, which is calculated:

$$\Delta i(s, t) = i(t) - p_L i(t_L) - p_R i(t_R) \quad (19)$$

where s is an index of possible thresholds, t is an index for the node in the classification tree, $i(t)$ is the impurity of the dataset before it is split at the node, $i(t_L)$ is the impurity of the subset of the data that goes to the left branch of the tree after the division, $i(t_R)$ is the impurity of the subset of the data that goes to the right branch after the division, and p_L and p_R are the portions of the dataset that are sent down the left and right branches of the tree, respectively. Ultimately, this condition aims to find the threshold that produces two pure subsets of the data. Several measures of impurity have been proposed [Breiman *et al.*, 1984]. One common measure is the so-called Gini index of diversity [Breiman *et al.*, 1984], which can be calculated:

$$i(t) = \sum_{j=1}^n p(t)_j [1 - p(t)_j] \quad (20)$$

where j is an index of the possible classifications (i.e. the five network types), n is the total number of possible classifications, and $p(t)_j$ is the portion of the networks in the dataset at t that belong to classification j .

Once the first split in the dataset is determined, each of the branches and their associated subsets of data are considered. New splits are determined separately for each of the branches that produce the least impure subsets. This procedure is continued until the full tree is developed. If the dataset is very complex, one usually needs to include a stopping condition after which further divisions of the data are ignored and some impurity in the resulting dataset is allowed.

Figure 5.4a shows the classification tree that was developed using all 50 of the drainage networks and the 9 variables described above. This tree is quite simple and successfully classifies all 50 drainage networks. The first condition it considers is the average value of the stream course irregularity measure. If this value is below a threshold value, then the network is either parallel or pinnate. Otherwise, it is dendritic, rectangular, or trellis. One can see why this measure was selected in Figure 5.2. The values for this measure fall within narrow ranges for any given network type, and parallel and pinnate networks have much lower values than the other networks. The classification method distinguishes between parallel and pinnate networks using the slope of the junction angle measure. From Figure 5.3, one can see that all the parallel networks have positive slopes whereas all of the pinnate networks have negative slopes. Rectangular networks are identified by considering the average stream course irregularity measure again. One can see from Figure 5.3 that rectangular networks have higher values for this measure than any other network type. Finally, the classification tree distinguishes dendritic and trellis networks by considering the average value of the drainage area increment measure. Figure 5.1 shows that trellis networks always have lower values than dendritic networks.

The classification tree in Figure 5.4a can be tested using a standard cross-validation procedure [Breiman *et al.*, 1984]. In this procedure, the 50 networks are divided into two groups, a training group consisting of 40 networks and a testing group consisting of 10 networks. The groups are selected randomly with the condition that the proportion of networks from each classification remains constant. Thus, the training group always has 8 networks from each classification, and the testing group always has 2 networks from each classification. The training group is used to develop the classification tree, and the tree is then used to predict the classifications of the 10 testing networks. We repeated the procedure using 50 randomly selected networks and found that the average number of misclassified networks is 0.7 out of 10, indicating that the classification method performs relatively well. It should also be noted that the structure of the classification tree is relatively robust. The variables used, the number of terminal nodes, and branches remain constant for the majority of the trees tested.

Although the tree in Figure 5.4a performs quite well, it does not strictly meet the objectives of the paper. In particular, significant slopes were observed for the parallel and pinnate network measures in Section 4, which we interpreted to be self-affinity. Thus, the average values of these measures are expected to depend on the scales of the parallel and pinnate networks. In order to develop a more scale invariant classification method, we explored the possibility of using the slopes of these measures by disallowing consideration of the average values of the parallel and pinnate networks. The classification tree is shown in Figure 5.4b. This classification method performs more poorly with the dataset we collected. Specifically, when developed from all 50 networks, it misclassifies 6 of the 50. In particular, two parallel networks are incorrectly identified

as trellis networks and four trellis networks are incorrectly identified as parallel networks. However, if one considered a dataset with a wider range of basin scales, this approach is expected to be superior because it is not dependent on scale.

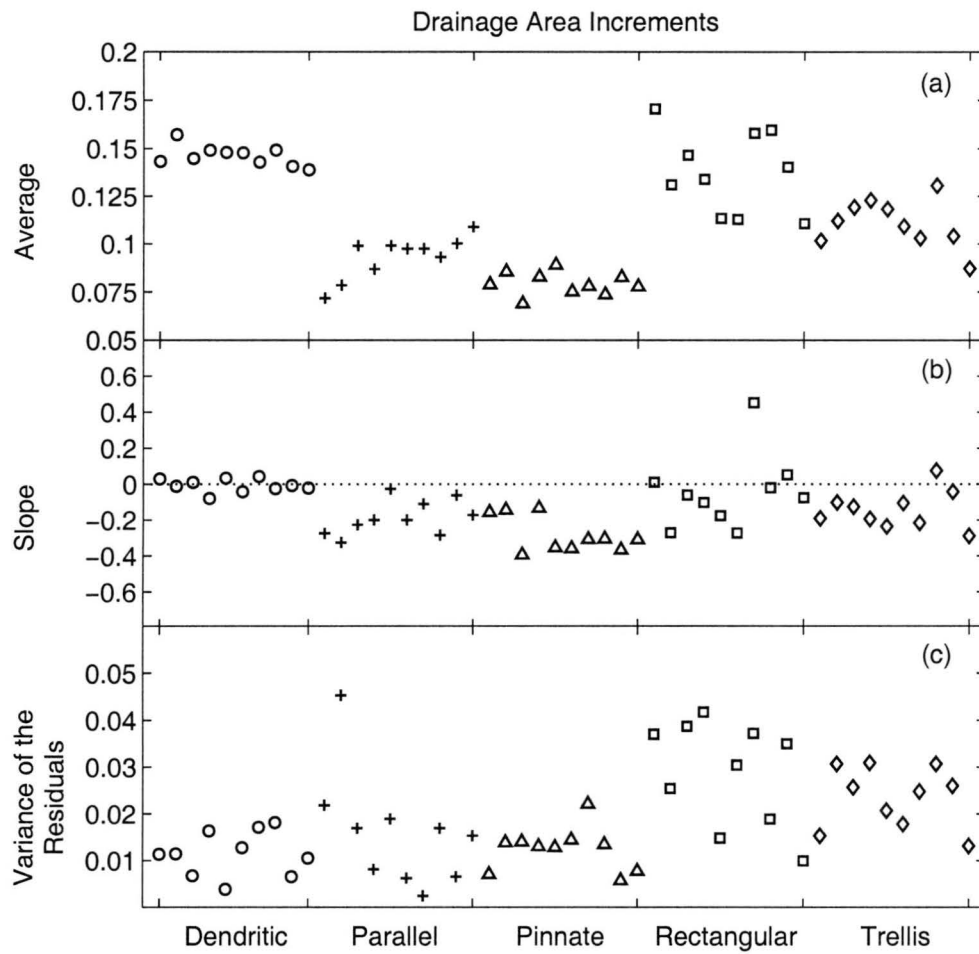


Figure 5.1. Summary of the average value, slope, and residual variance obtained for the drainage area increments.

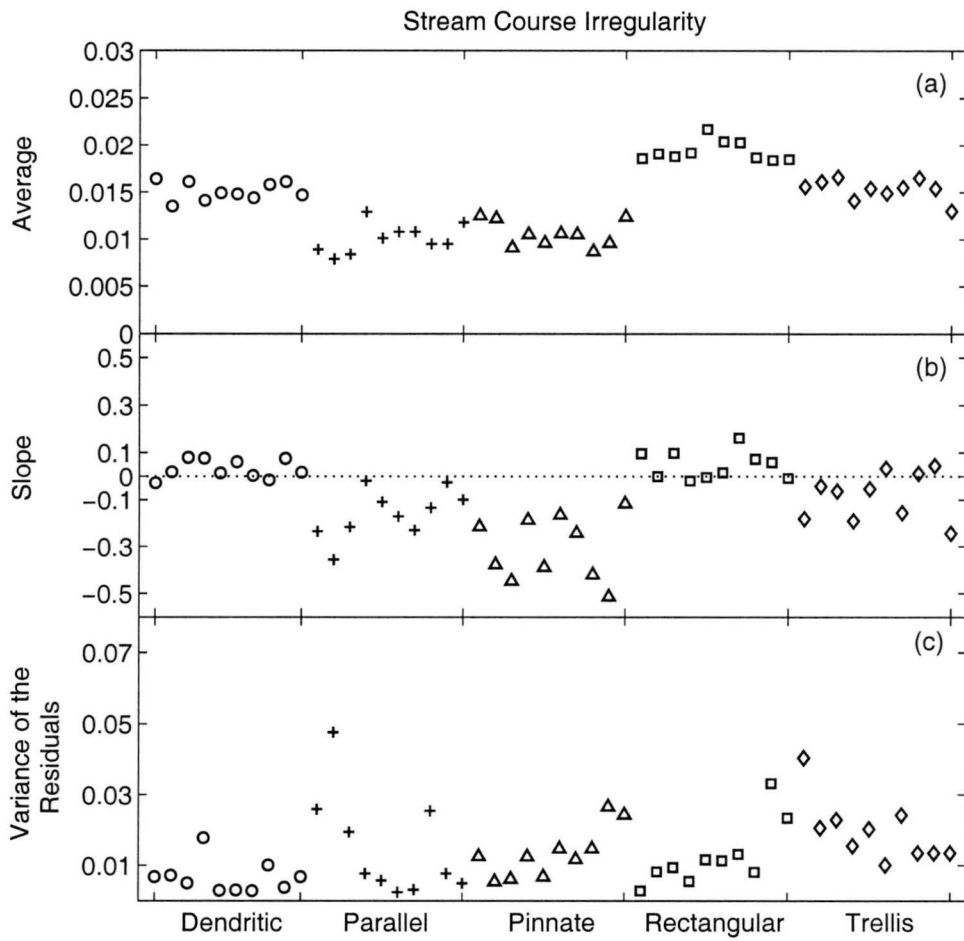


Figure 5.2. Summary of the average value, slope, and residual variance obtained for the stream course irregularity.

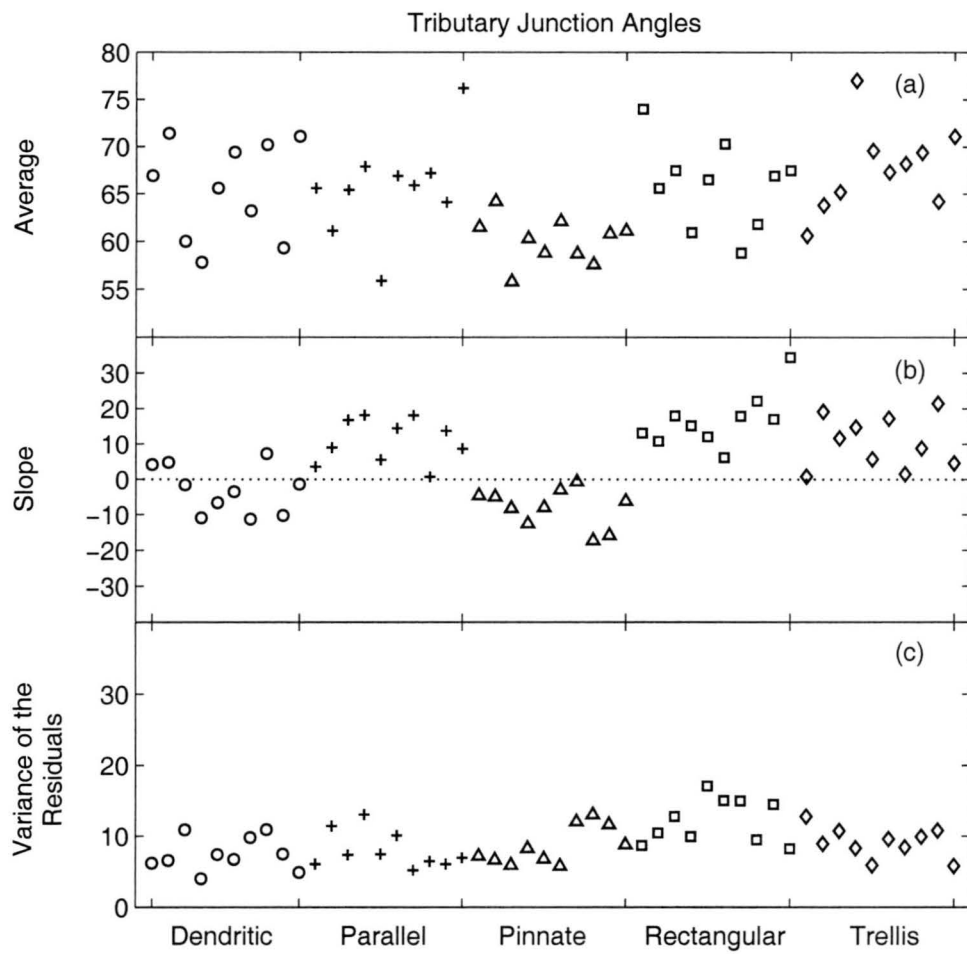


Figure 5.3. Summary of the average value, slope, and residual variance obtained for the tributary junction angles.

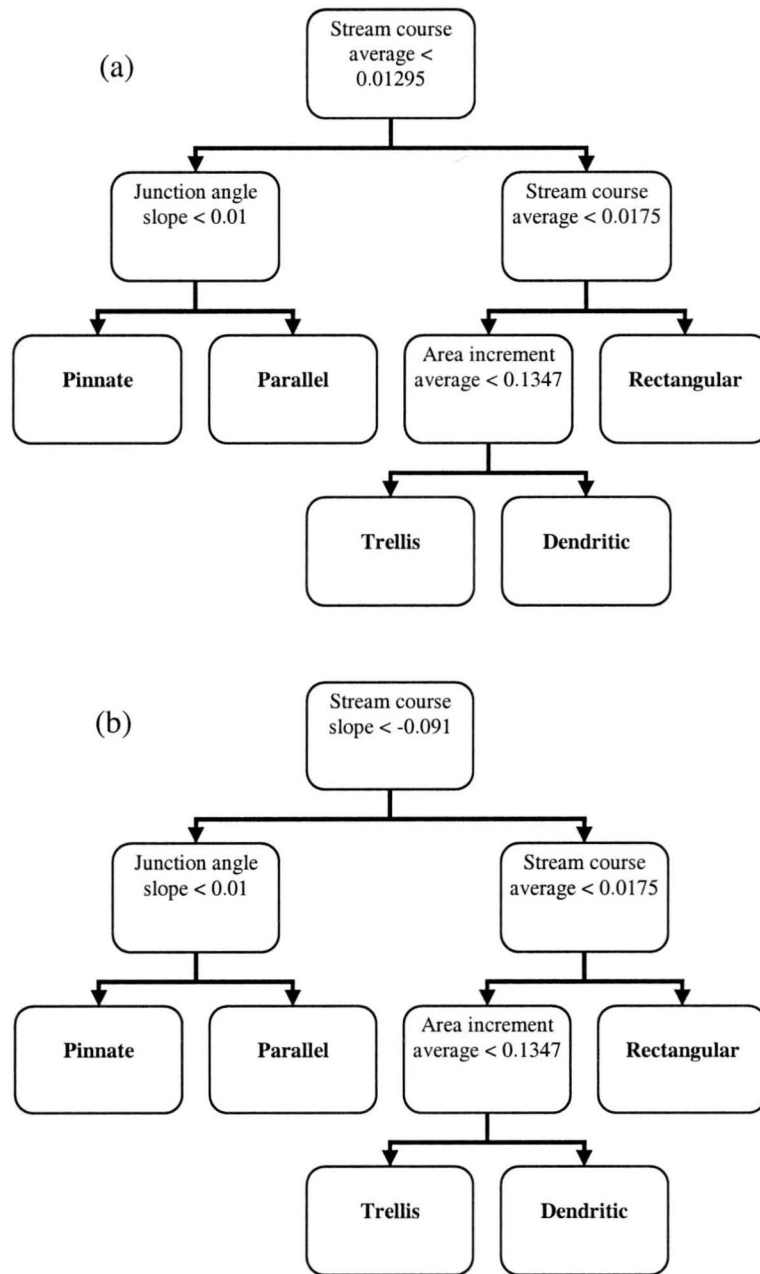


Figure 5.4. (a) Automatically-generated and (b) conceptual classification trees derived from all 50 basins analyzed in this paper.

6 Conclusions

In this paper, we attempted to distinguish dendritic, parallel, pinnate, rectangular, and trellis networks using three measures of network properties derived from planform self-similarity. Based on this analysis, we can conclude the following:

1. The planform characteristics of dendritic networks conform to self-similarity as suggested by previous authors. The self-similarity in the drainage area increments is the most robust, while the self-similarity of the junction angles is least robust among the measures considered.
2. The planform features of parallel networks are self-affine. The average estimate for the Hurst exponent is 0.81 using the drainage area increments and 0.84 using the stream course irregularity. The self-affinity suggests that large parallel basins accumulate less drainage area and have less stream course irregularity in comparison to their size than small basins. These results offer a quantification of the response of drainage networks to an imposed regional slope, which could be used to test long-term erosion models.
3. The planform features of pinnate networks also exhibit self-affinity. The drainage area increments produce an average estimate of H around 0.72, while the stream course irregularity produces an average estimate of 0.69. These results suggest that pinnate networks are more self-affine than parallel networks.
4. Rectangular networks are best approximated by self-similarity, although deviations are observed in all three of the measures used in this paper. The normalized stream

course irregularity for all the rectangular networks analyzed is larger than the irregularity for any of the other networks considered. The increase in sinuosity that is observed in response to jointing in the underlying bedrock represents another pathway that could be used to test and improve long-term fluvial erosion models.

5. Like rectangular networks, trellis networks are approximately self-similar, although deviations are observed in all three measures. The deviations for trellis networks tend to occur over broader ranges of basin sizes than those for rectangular networks and might produce some degree of self-affinity. The most distinguishing feature of trellis networks is the reduced average value of the drainage area increment measure. This result suggests that trellis networks accumulate drainage area at a slower rate than dendritic networks, or equivalently are more elongated than dendritic networks.

6. A classification tree was developed using the average, slope, and residual variance for the regression lines fitted to the three measures. If this classification tree is allowed to use the average values for the stream course irregularity for all network types, it successfully classifies all of the networks. However, the use of this measure for self-affine networks renders the method scale dependent. If the use of these measures is disallowed, then the classification is scale invariant but it successfully classifies only 44 out of 50 networks. Both of the trees developed here are much simpler than those used in previous quantitative classification methods.

References

- Abrahams, A. D., and J. J. Flint (1983), Geologic controls on the topological properties of some trellis channel networks, *Geological Society of America Bulletin*, 94, 80-91.
- Argialas, D. P., J. G. Lyon, and O. W. Mintzer (1988), Quantitative description and classification of drainage patterns, *Photogrammetric Engineering and Remote Sensing*, 54, 505-509.
- Balk, B., and K. Elder (2000), Combining binary decision tree and geostatistical methods to estimate snow distribution in a mountain watershed, *Water Resources Research*, 36, 13-26.
- Bittencourt, H. R., and R. T. Clarke (2004), Feature selection by using classification and regression trees (CART), in *XXth ISPRS Congress*, edited, Istanbul, Turkey.
- Breiman, L., J. H. Friedman, R. A. Olshen, and C. J. Stone (1984), *Classification and Regression Trees*, Wadsworth, Inc., Belmont, California.
- Burbank, D. W. (1992), Causes of recent Himalayan uplift deduced from deposited patterns in the Ganges basin, *Nature*, 357, 680-683.
- Cox, K. G. (1989), The role of mantle plumes in the development of continental drainage patterns, *Nature*, 342, 873-877.
- Daniel, J. R. K. (1981), Drainage density as an index of climate geomorphology, *Journal of Hydrology*, 50, 147-154.
- De'ath, G., and K. E. Fabricius (2000), Classification and regression trees: a powerful yet simple technique for ecological data analysis, *Ecology*, 81, 3178-3192.
- De Serres, B., and A. G. Roy (1990), Flow direction and branching geometry at junctions in dendritic river networks, *The Professional Geographer*, 42, 194-201.
- Dodds, P. S., and D. H. Rothman (1999), Unified view of scaling laws for river networks, *Physical Review E*, 59, 1-15.

- Dunne, T. (1980), Formation and controls of channel networks, *Progress in Physical Geography*, 4, 211-239.
- Flint, J. J. (1974), Stream gradient as a function of order, magnitude, and discharge, *Water Resources Research*, 10, 969-973.
- Gómez-Chova, L., J. Calpe, E. Soria, G. Camps-Valls, J. D. Martín, and J. Moreno (2003), CART-based feature selection of hyperspectral images for crop cover classification, paper presented at IEEE International Conference on Image Processing, IEEE Computer Society Press, Barcelona, Spain.
- Gregory, K. J., and D. E. Walling (1973), *Drainage Basin Form and Process: a geomorphological approach*, Edward Arnold, London.
- Gupta, V. K., and E. C. Waymire (1993), A statistical analysis of mesoscale rainfall as a random cascade, *Journal of Applied Meteorology*, 32, 251-267.
- Hack, J. T. (1957), Studies of longitudinal profiles in Virginia and Maryland, *U.S. Geological Survey Professional Paper*, 294-B.
- Horton, R. E. (1932), Drainage-basin characteristics, *Transactions of the American Geophysical Union*, 13, 350-361.
- Horton, R. E. (1945), Erosional development of streams and their drainage basins; hydrophysical approach to quantitative morphology, *Bull. Geol. Soc. Am.*, 56, 275-370.
- Howard, A. D. (1967), Drainage analysis in geologic interpretation: a summation, *The American Association of Petroleum Geologists Bulletin*, 51, 2246-2259.
- Howard, A. D. (1971), Optimal angles of stream junction: geometric, stability to capture, and minimum power criteria, *Water Resources Research*, 7, 863-873.
- Howard, A. D. (1994), A detachment-limited model of drainage basin evolution, *Water Resources Research*, 30, 2261-2285.
- Ichoku, C., and J. Chorowicz (1994), A numerical approach to the analysis and classification of channel network patterns, *Water Resources Research*, 30, 161-174.
- Jaynes, D. B., T. C. Kaspar, T. S. Colvin, and D. E. James (2003), Cluster analysis of spatiotemporal corn yield patterns in an Iowa field, *Agronomy Journal*, 95.
- Knighton, D. (1998), *Fluvial Forms and Processes, a new perspective*, First edition ed., Arnold, London.

- Lubowe, J. K. (1964), Stream junction angles in the dendritic drainage pattern, *American Journal of Science*, 262, 325-339.
- Maling, D. H. (1992), *Coordinate Systems and Map Projections*, 2nd ed., Pergamon Press, New York.
- Milton, L. (1965), Quantitative expression of drainage net patterns, *Australian Journal of Science*, 27, 238-240.
- Montgomery, D. R., and W. E. Dietrich (1992), Channel initiation and the problem of landscape scale, *Science*, 255, 826-830.
- Montgomery, D. R., and E. Foufoula-Georgiou (1993), Channel networks source representation using digital elevation models, *Water Resources Research*, 29, 3925-3934.
- Morisawa, M. E. (1963), Distribution of stream-flow direction in drainage patterns, *Journal of Geology*, 71, 528-529.
- Muñoz, J., and A. M. Felicísimo (2004), Comparison of statistical methods commonly used in predictive modeling, *Journal of Vegetation Science*, 15, 285-292.
- Niemann, J. D., and L. E. Hasbargen (2005), A comparison of experimental and natural drainage basin morphology across a range of scales, *Journal of Geophysical Research*, 110, F04017.
- O'Callaghan, J. F., and D. M. Mark (1984), The extraction of drainage networks from digital elevation data, *Computer Vision, Graphics and Image Processing*, 328-344.
- Parvis, M. (1950), Drainage pattern significance in airphoto identification of soils and bedrocks, *Photogrammetric Engineering*, 16, 375-409.
- Peckham, S. D. (1995), New results for self-similar trees with applications to river networks, *Water Resources Research*, 31, 1023-1029.
- Perse, S. J. (1960), Speech at the Nobel Prize Banquet, Stockholm, Sweden.
- Phillips, L. F., and S. A. Schumm (1987), Effect of regional slope on drainage networks, *Geology*, 15, 813-816.
- Pieri, D. C. (1984), Junction angles in drainage networks, *Journal of Geophysical Research*, 89, 6878-6884.
- Plummer, C. C., and D. McGeary (1993), *Physical Geology*, Sixth edition ed., 537 pp., Wm. C. Brown, Dubuque, IA.

- Rigon, R., I. Rodríguez-Iturbe, A. Maritan, A. Giacometti, D. G. Tarboton, and A. Rinaldo (1996), On Hack's law, *Water Resources Research*, 32, 3367-3374.
- Rodríguez-Iturbe, I., E. Ijjasz-Vásquez, R. L. Bras, and D. G. Tarboton (1992), Power law distributions of mass and energy in river basins, *Water Resources Research*, 28, 988-993.
- Schertzer, D., and S. Lovejoy (1987), Physical modelling and analysis of rain and clouds by anisotropic scaling multiplicative processes, *Journal of Geophysical Research*, 92, 9693-9714.
- Schumm, S. A. (1956), Evolution of drainage systems and slopes in badlands at Perth Amboy, *Bulletin of the Geological Society of America*, 67, 597-646.
- Strahler, A. N. (1957), Quantitative analysis of watershed geomorphology, *EOS Transactions AGU*, 38, 913-920.
- Tarboton, D. G., R. L. Bras, and I. Rodríguez-Iturbe (1991), On the extraction of channel networks from digital elevation data, *Hydrological Processes*, 5, 81-100.
- Van Sickle, J. (2004), *Basic GIS coordinates*, CRC Press, Boca Raton.
- Vayssières, M. P., R. E. Plant, and B. H. Allen-Díaz (2000), Classification trees: an alternative non-parametric approach for predicting species distributions, *Journal of Vegetation Science*, 11, 679-694.
- Veneziano, D., and J. D. Niemann (2000a), Self-similarity and multifractality of fluvial erosion topography: 1. Mathematical conditions and physical origin, *Water Resources Research*, 36, 1923-1936.
- Veneziano, D., and J. D. Niemann (2000b), Self-similarity and multifractality of fluvial erosion topography: 2. Scaling properties, *Water Resources Research*, 36, 1923-1936.
- White, R. L. (1997), Object classification in astronomical images, in *Statistical Challenges in Modern Astronomy II*, edited by G. J. Babu and E. D. Feigelson, pp. 135-148, Springer, New York.
- Zernitz, E. R. (1932), Drainage patterns and their significance, *Journal of Geology*, 40, 498-521.